ARMY RESEARCH LABORATORY

Fin Damage and Rod Eccentricity for Spin/Pitch Lock-in for Antiarmor Kinetic Energy Projectiles

Ameer G. Mikhail

ARL-TR-1442 NOVEMBER 1997

Army Research Laboratory
Aberdeen Proving Ground, MD 21005-5066

ARL-TR-1442 November 1997

Fin Damage and Rod Eccentricity for Spin/Pitch Lock-in for Antiarmor Kinetic Energy Projectiles

Ameer G. Mikhail
Weapons & Materials Research Directorate

Abstract

A study and a general model for the roll/pitch frequency “lock-in” phenomenon are made for antitank long kinetic energy projectiles and missiles in general, to quantify the necessary projectile damage/defect required to cause the lock-in. (Lock-in is a “persistent” resonance for the flight duration of the vehicle [i.e., projectile].) Fin damage and body mass offset are modeled as the forcing forces and moments (asymmetries) causing the lock-in. Idealized fin damage is modeled. The corresponding pitch, side slip, and roll equations are numerically integrated. The resulting yaw is largest when the projectile is spinning near the pitching frequency, and the yaw diminishes when the spin rate (attributable to fin damage) is far from it. The nonlinear induced roll moment is essential in coupling the pitching and yawing motions with the rolling motion. A specific and complete projectile case study is presented, in which quantified fin damage and rod mass offset are found to cause such lock-in. Computed flight motion history (pitch, side slip, and roll), and yaw amplification factor provide insight into this lock-in behavior. The model is general and can be applied to any finned projectile or missile.

TABLE OF CONTENTS

INTENTIONALLY LEFT BLANK

LIST OF FIGURES

INTENTIONALLY LEFT BLANK

LIST OF TABLES

INTENTIONALLY LEFT BLANK

FIN DAMAGE AND ROD ECCENTRICITY FOR SPIN/PITCH LOCK-IN FOR ANTIARMOR KINETIC ENERGY PROJECTILES

1. INTRODUCTION

Long antitank kinetic energy (KE) projectiles and missiles are known to occasionally exhibit abnormal flight behavior characterized by (a) spinning at a different rate than their intended design values, and (b) having larger than expected yawing motion angles. In fewer cases, this behavior can be catastrophic to the motion and mission of the vehicle, causing an ineffective armor penetration for the KE projectile case, or uncontrollable flight for the missile case. Note that the projectile flight duration is only 1 to 3 seconds.

When these two events occur, it is most likely that a roll/pitch "lock-in" has occurred where the "vehicle" (i.e., projectile/missile) inappropriately spins because of damaged fins or other asymmetry, close to the pitching motion frequency of the vehicle. This fin damage is usually referred to in the literature as "asymmetries," which are suffered by the vehicle. Lock-in is a "persistent" resonance for the flight duration of the vehicle. Figure 1 shows a fin impact imprint indicating damaged parts of two fins[1], bent by angles exceeding 30°. Also, a KE projectile impact imprint[2] at 3 km indicates large yaw angle, estimated here at about 8.8°.

This roll/pitch lock-in phenomenon is not new and has been studied by many researchers since the late 1940's. Nicolaides[3] provided an early analysis while Price[4] provided a useful and practical model for the mechanisms causing the phenomenon. Clare[5,6] provided the effect of nonlinearities on such motion. Murphy included the asymmetries in his formulation[7] and later showed[8] that lock-in can happen at a reverse spin rate. More recently, Lin et al.[9] studied this problem for a re-entry vehicle (with no fins) and considered longitudinal body curvature attributable to flexure as part of the total angle of attack, in a zeroth order model for flexure effects. For more prior art, the reader is referred to References 4, 5, 8, and 9, which together, list about 186 references covering this lock-in behavior and its model development over the years.

The design spin for a KE projectile or a missile has to avoid being close to the natural pitching motion frequency or to the first natural lateral bending frequency of the vehicle. For the KE projectile shown in Figure 2, the former is about 24 Hz (decreases from 25 to 23) while the latter (for the steel model herein) was about 385 Hz. The design

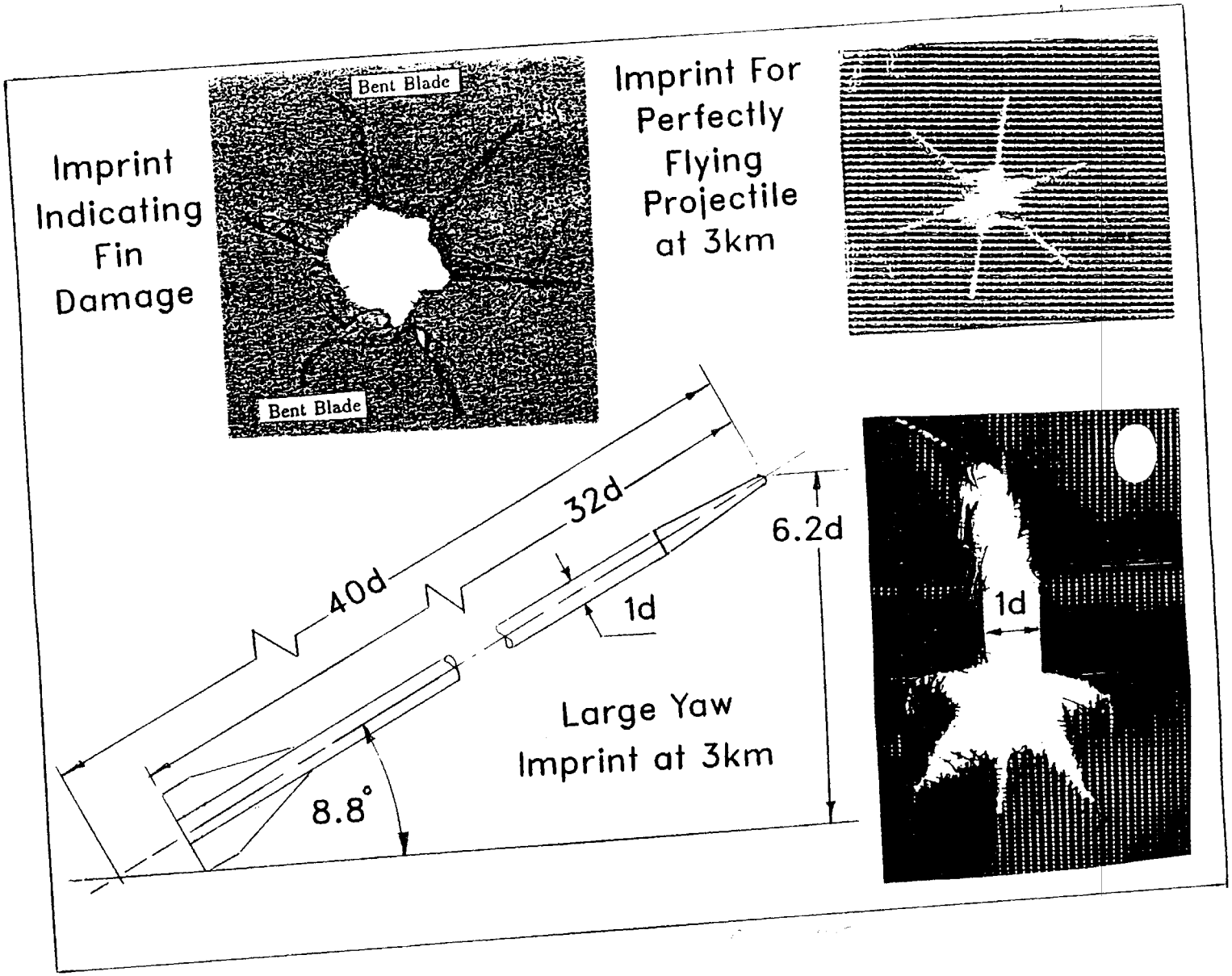

Figure 1. Observed Damaged Fins and Large Yaw for a KE Projectile.

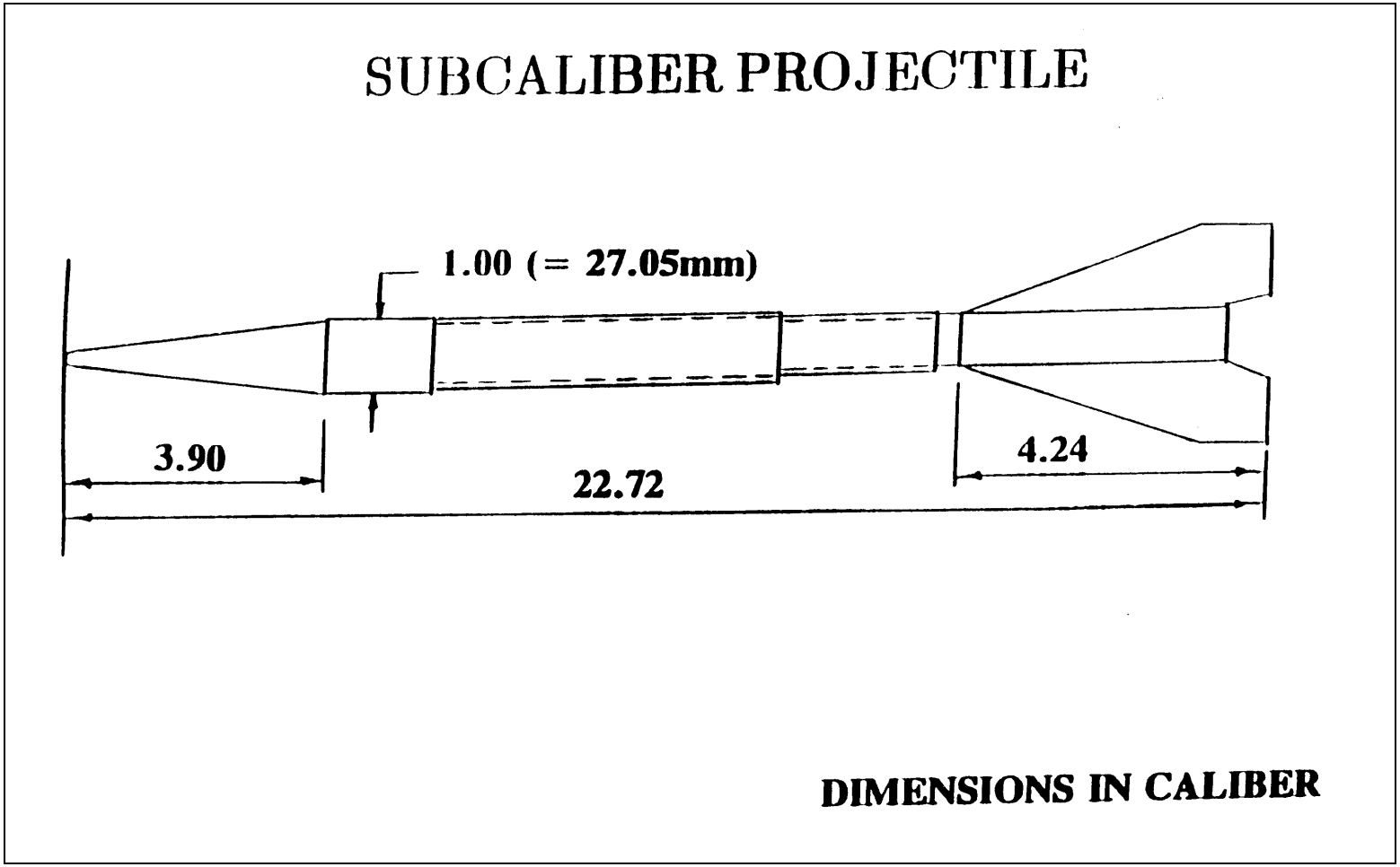

Figure 2. Geometry of the 120-mm M829 Subcaliber KE Projectile.

spin for that projectile is 90 Hz, as depicted in Figure 3. Certain fin damage can cause the projectile to underspin its design value and spin near its pitching frequency, as shown in Figure 4. These particular spin values near this pitching motion frequency are studied in detail later in this report. In Reference 10, the spin lock-in with the upper frequency limit (the first bending frequency) attributable to structural causes was studied and reported. In the present lock-in phenomenon, the mechanisms for causes are dynamic motion related to the pitching and side slip angles coupled to a lower roll rate attributable to fin damage. The present study concerns lock-in at this lower limit, its implication, and the motion instability amplification it induces. Reference 11 provides results for pitch lock-in with rod flexure but gives no details about the exact formulation, equations, or roll information, including any induced roll moment.

Usually, "roll" implies a low spin value. Historically, it came from the aeronautical reference to aircraft roll rate. Spin, however, indicates high value of roll. Commercial aircraft may roll only few degrees to bank, while a military aircraft may do a few complete rolls for maneuver. Missiles usually have low roll rate (1 to 5 Hz), while finned projectiles "spin" at 50 to l50 Hz, and unfinned projectiles may be spun to more than 300 Hz. In the present work, the spin/pitch lock-in is occasionally called roll/pitch lock-in, as it is frequently called in the literature.

The present work adapts the work of Price[4] to the formulation of Reference 7. Numerical solutions will be obtained for the three coupled roll/pitch/side slip equations. A case study is made for the 120-mm M829 steel version of the projectile. Flight histories and impact imprints are presented under different fin damage and mass offset values.

2. ANALYSIS

2.1 Definitions

Resonance between the roll and pitching frequencies is defined as when the former is affected by the value of latter, when the two values nearly match each other. Roll lock-in is when the former frequency attains and maintains the value of the latter for a long and persistent time (1 to 3 seconds for KE projectiles; many seconds or minutes for a missile). Vehicles can roll resonate when crossing the pitching frequency but may not lock in to it. Vehicles that roll lock-in must resonate with the pitch frequency. However, vehicles may temporarily lock in but then escape later, in what might be called "a prolonged resonance."

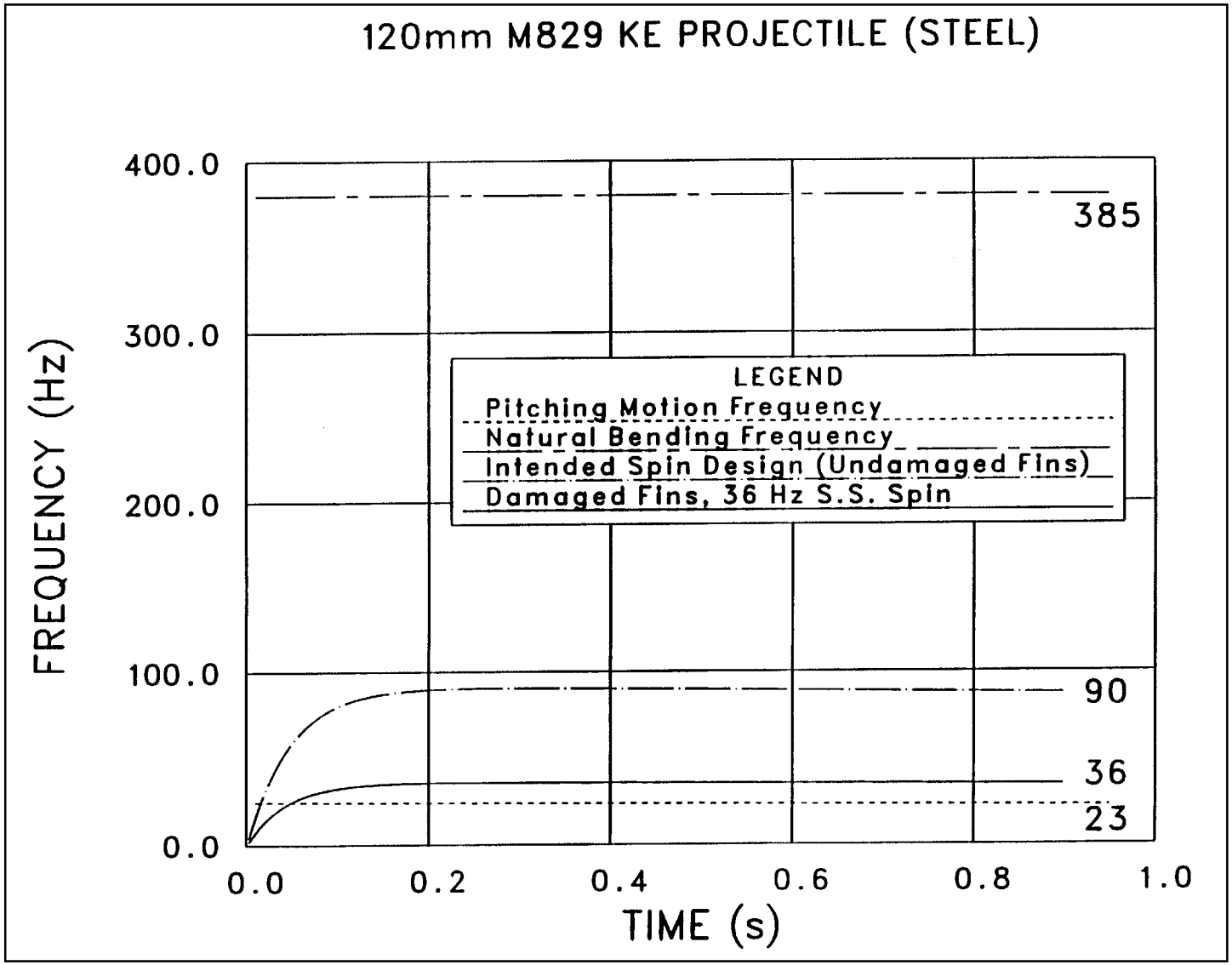

Figure 3. Design Spin (undamaged fins) Falling Between the Two Limiting Frequencies.

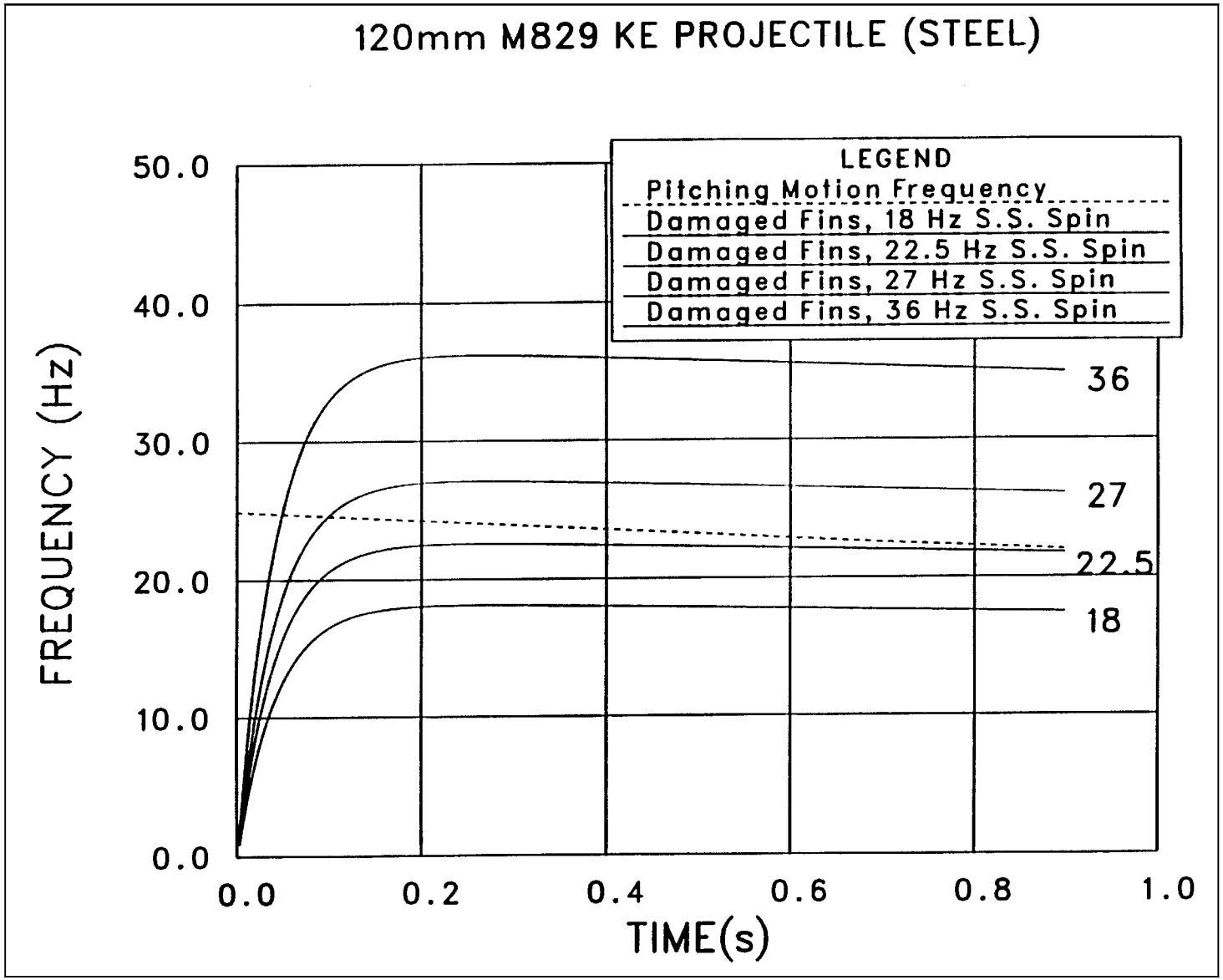

Figure 4. Spin Cases Studied Near the Pitching Frequency (undamaged fins).

Yaw angle is the side slip angle, β. The yawing motion is therefore the motion in the yaw plane. However, it is common in ballistics to refer to the total angle of attack as the "yaw" angle and the total motion as the "yawing" motion. In the present work, yaw refers to the correct side slip definition.

2.2 Induced Roll Moment

The induced roll moment, C_{li}, is generated on a finned vehicle because of the cyclic fin loading at different angles of attack. Its magnitude is a function of both the fin orientation angle during roll (with respect to a reference plane) and with the total angle of attack. It is nonlinear (sinusoidal) with the fin orientation angle and nonlinear with the total angle of attack, although it is also small for small α. More importantly, it links (i.e., couples) the yawing motion to the roll motion. Reference 4 only cites a case of the wind tunnel experiment of the Aerobee 150A sounding rocket, but the actual test values are provided in Reference 5 (which provides more details about the analytic form of that coefficient). C_{li} is defined as

$$C_{li} = induced\ roll\ moment/(qA_{ref}\, d\, sin(n\gamma)) \tag{1}$$

Clare[5] provides a useful algebraic fit based on the experimental testing of the Basic Finner. He applied the same expression to the Apache missile, and Price[4] applied it to the Aerobee rocket.

$$C_{li} = (-0.87 + 17.9\alpha_t^2)\alpha_t \tag{2}$$

The same pattern of variation with α_t was also observed for the Basic Finner (code name) projectile and is given in Reference 12. It is interesting to notice that both cases exhibit a negative value until $\alpha_t = 12.6^\circ$ and then become rapidly positive. This measured behavior was not observed or used in Reference 8 which uses a simplistic C_{li} algebraic sixth order variation with α_t for a six-finned projectile configuration. Clare also used the C_{li} values of the Basic Finner for his Apache missile configuration, which is generally similar in shape to both the Basic Finner and the M829 projectile used here. In the present work, the expression of Equation (1) for the Basic Finner will be used for the M829 projectile since no data are available for the latter.

2.3 Mechanisms for Lock-in

Reference 4 lists three main missile asymmetry categories that can cause lock-in. First is configuration asymmetries such as fin cant manufacturing tolerance, fin damage during launch or in-flight, or a bent nose, each of which results in a static trim angle. Rocket thrust misalignment with the body axis is another example. Second is the mass center location deviation from the body axis, which provides coupling of the roll with the aerodynamic normal force of the vehicle. Third is the aerodynamic-geometric interactions such as the fin rotation-angle of attack interaction causing the induced roll moment described earlier. Elastic bodies that can bend or deform, thus causing a change in the aerodynamic forces from their intended design values, are another example.

2.4 Formulation

2.4.1. *Analysis of Price (Rolling Coordinates)*

Price[4] adapted the yaw and pitch equations developed earlier by Nielson for a constant spin case, to accept varying spin rates. The equations of Nielson (cited in Reference 4) for pitch and yaw angles were written in body-fixed coordinates, i.e., rolling with the body itself. Price then added the roll equation and included the induced roll moment. He also added the terms for the effects of mass offset, moment asymmetry, and rocket thrust misalignment to the three equations. The latter effect will not be considered in the present work. The general nomenclature and coordinates are shown in Figure 5. The roll motion equation with the added mass offset, Δcg, and the induced roll moment was written by Price as

$$I_x \ddot{\phi} = q.A_{ref}.d.(C_{l\delta}.\delta + C_{lp}\frac{\dot{\phi}d}{V} - C_{li}.sin(n\bar{\phi}) - \frac{\Delta cg}{d}.C_{N\alpha}.\alpha_{trim}.sin(\bar{\phi}-\Gamma)) \qquad (3)$$

subject to the initial condition

$$\phi = \phi_o \qquad at \quad t = 0, \qquad (4)$$

in which

$$\dot{\phi} \equiv d\phi / dt = p$$

$$\psi = tan^{-1}\left[\frac{b\,p/\omega_p}{1.-p^2(1.-Ix/Iy)/\omega_p^2}\right]$$

$$\bar{\phi} = \lambda - \psi$$

$$b = \left(qA_{ref} / mV\omega_p\right)\left(C_{N\alpha}\left[1. - I_x / I_y\right] - md^2 C_{Mq} I_y\right).$$

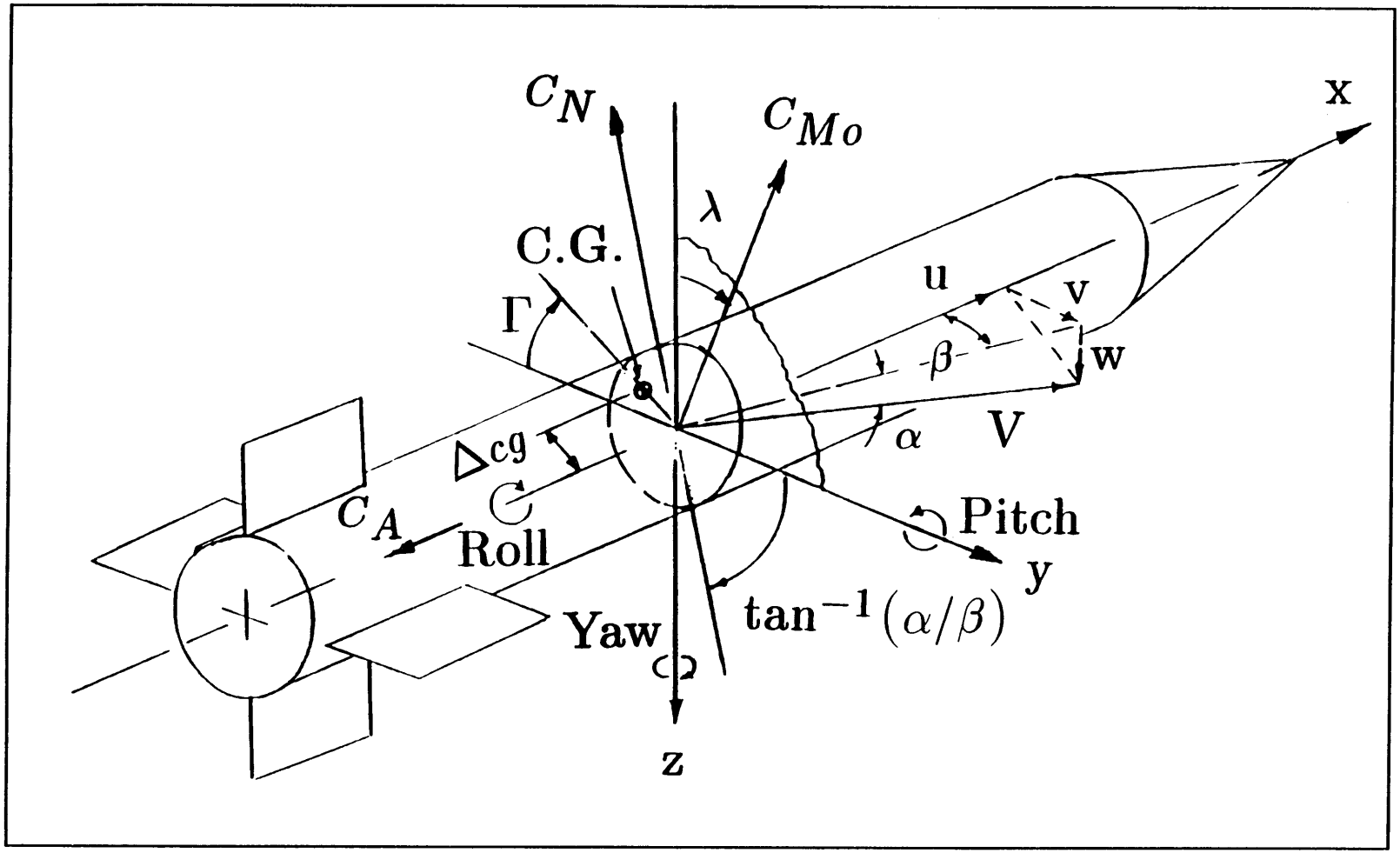

Figure 5. Nomenclature, Coordinates, and Angles (after Price[4]).

Also, $-\psi$ is the phase angle, and $\bar{\phi}$ is the fin orientation angle. The sin( ) in Equation (3) represents the variation with the roll angle for each of C_{li} and the mass offset roll moment. Note that the assymetry pitching moment does not show up explicitly in the roll Equation (3), except through the C_{li} term which reflects the values of α and β, which in turn are affected by C_{Mo}.

2.4.2. *Non-Rolling Coordinates*

The analysis of Reference 7 is almost standard in ballistics formulation. It uses a ballistic coordinate system (i.e., axes are attached to the center of gravity [CG] of the body and move with it but do not roll with the body). Reference 7 has the standard form which was expanded here in the α, β, and time variables, modified for the added asymmetry effects, and re-written in Price's form:

$$\ddot{\beta} + A_1 \dot{\beta} - A_2 \dot{\alpha} - B_1 \beta + B_2 \alpha = C_1 \tag{5}$$

$$\ddot{\alpha} + A_1 \dot{\alpha} + A_2 \dot{\beta} - B_1 \alpha - B_2 \beta = C_2 \tag{6}$$

in which

$A_1 = (qA_{ref}/mV)(C_{L\alpha} - md^2[C_{Mq} + C_{M\dot{\alpha}}]/I_y)$

$A_2 = -P(I_x/I_y)$

$B_1 = (qA_{ref}\, d/I_y)C_{M\alpha}$

$B_2 = (pqA_{ref}/mV)(C_{L\alpha} I_x/I_y + md^2/I_y\, C_{Mp\alpha})$

$C_1 = (qA_{ref}\, d/I_y)(C_{Mo} \cos[\lambda + \phi] - C_A \frac{\Delta cg}{d} \cos[\Gamma + \phi])$

$C_2 = (qA_{ref}\, d/I_y)(C_{Mo} \sin[\lambda + \phi] - C_A \frac{\Delta cg}{d} \sin[\Gamma + \phi])$

$C_{Mp\alpha}$ = Magnus moment slope coefficient, Magnus moment/$(qA_{ref}\, d[pd/V]\alpha)$

$(C_{Mq} + C_{M\dot{\alpha}})$ = pitch moment damping coefficient, pitch damping moment/$(qA_{ref}\, d[\hat{q}\, d/V])$

$\hat{q}$ = local pitching rate

m = mass of projectile.

The λ angle is such that $C_{Moz} = C_{Mo}\cos(\lambda)$ and $C_{Moy} = C_{Mo}\sin(\lambda)$. The pitch angle, α, is positive when the vehicle nose is up, while C_M (hence, $C_{M\alpha}$) is negative when it turns the nose tip down. Without C_1 and C_2 in Equations (5) and (6), both α and β equations will have ω_p as their natural frequency.

The roll equation [Equation (3)] is modified for the non-spinning axes and re-written after Price's model. The modification is to reflect the tracking of the roll angle in non-rolling coordinates. The angles of rotation are tracked from a reference plane taken to be the vertical.

$$I_x \ddot{\phi} = q.A_{ref}.d.(C_{l\delta}.\delta + C_{lp}\frac{\dot{\phi}d}{V} - C_{li}.sin(n\bar{\phi}) - \frac{\Delta cg}{d}.C_{N\alpha}.\alpha_t.sin[\phi + \Gamma - \hat{\phi}])$$

(7)

in which

$\bar{\phi}$ = $(\phi + \phi_o - \hat{\phi})$

ϕ = roll angle, measured from a fixed reference plane

ϕ_o = initial roll angle, measured from same reference plane

$\hat{\phi}$ = $tan^{-1}(\beta/\alpha)$, pitching motion plane, measured from same reference plane

in which $\bar{\phi}$ is the the angle between the pitch plane and the fin orientation angle. The yaw amplification factor for the trim angle of attack, based on Reference 7 for symmetric missiles with small yaw angles and linear aerodynamics, is usually written as[13]

$$AMP = \frac{\alpha_t}{\alpha_{trim\ at\ zero\ spin}} = \frac{-0.5\rho\ A_{ref}\,d\,C_{M\alpha}}{I_y\sqrt{\left[\left(\{\bar{p} - \acute{\phi}_f\}\{\bar{p} - \acute{\phi}_s\} - \lambda_f\lambda_s\right)^2 + \left(\lambda_s\{\bar{p} - \acute{\phi}_f\} + \lambda_f\{\bar{p} - \acute{\phi}_s\}\right)^2\right]}}$$

in which

$\bar{p}$ = p/V

$\dot{\phi}_f$ = $\bar{p}\,I_x(1. + \sigma)/(2I_y)$

$\dot{\phi}_s$ = $\bar{p}\,I_x(1. - \sigma)/(2I_y)$

σ = $\sqrt{1. - 1./S_g}$

S_g = $2I_x^2\bar{p}^2 / (\pi I_y \rho C_{M\alpha} d^3)$

λ_f = $\frac{\rho A_{ref}}{4m}\left[-C_{N\alpha}(1. - 1./\sigma) + 0.5k_2(1. + 1./\sigma)C_{Mq} + k_1 C_{Mp\alpha}/\sigma\right]$

λ_s = $\frac{\rho A_{ref}}{4m}\left[-C_{N\alpha}(1. + 1./\sigma) + 0.5k_2(1. - 1./\sigma)C_{Mq} - k_1 C_{Mp\alpha}/\sigma\right]$

k_1 = md^2/I_x

k_2 = md^2/I_y

This amplification factor represents the ratio of the steady state yaw angle of a spinning projectile to the corresponding steady state yaw angle of a corresponding non-spinning projectile (i.e., projectile in combined pitching and yawing motions only). In the present study, however, the time-dependent growth history in the yaw angle (in reference to the initial total yaw angle at launch) is introduced in Section 5. This new amplification factor time history is also given in Section 5.

2.4.3 *Fin Damage*

In ballistics practice, damage to fins may be observed on x-ray or video films taken for projectiles exiting the muzzle. Some fin damage is only realized when yaw tests (using yaw cards) are performed. However, fin damage cannot be predicted *a priori*. Most fin damage occurs in the gun tube and before the projectile exits the muzzle (some damage because of aeroheating may occur during flight), as was also recently ascertained in Reference 14. Seldom are the fins recovered after each firing to examine the damage. In many cases, fin damage could only be assumed, based on untypical flight performance such as large yaw angles at large ranges (1 to 3 km for projectile applications) or a screen impact imprint indicating rod bending or even missing or bent fins. Unfortunately, for those observed flight abnormalities, no fin damage was expected nor were the fins recovered. Therefore, theoretical studies and models, like the present work, are used to explain the relation between the abnormal flight behavior (e.g., roll/pitch lock-in or roll/flexure lock-in) and possible fin damage. A question is often posed about how much and what type of fin damage it takes to cause such behavior, even if the damage itself cannot be prevented. The present work sheds some light in that respect. Theoreticians[8] assign numerical values to "asymmetries," but they never relate these to real-life fin damage and examine if those values are realistic.

In the present study, fin damage is idealized into three types that are most often observed from yaw card tests. Corresponding damaged fin areas of 5% and 10% for a single fin panel bent at different damage angles are studied as a practical example. The fin damage cannot be just arbitrarily assumed in size and direction but must be made consistent to explain the loss in roll rate from its design value as well. Therefore, only damage in a certain direction relative to the fin cant angle and spin direction can be applied. Although other fin angle damage directions obviously happen, they will not result in lower roll and, thus, in this spin/pitch lock-in. In fact, Reference 10 purposefully considered the reverse case only (i.e., only damage that will overspin the projectile) to study the spin/flexure lock-in behavior. Figure 6 shows the required fin damage direction to

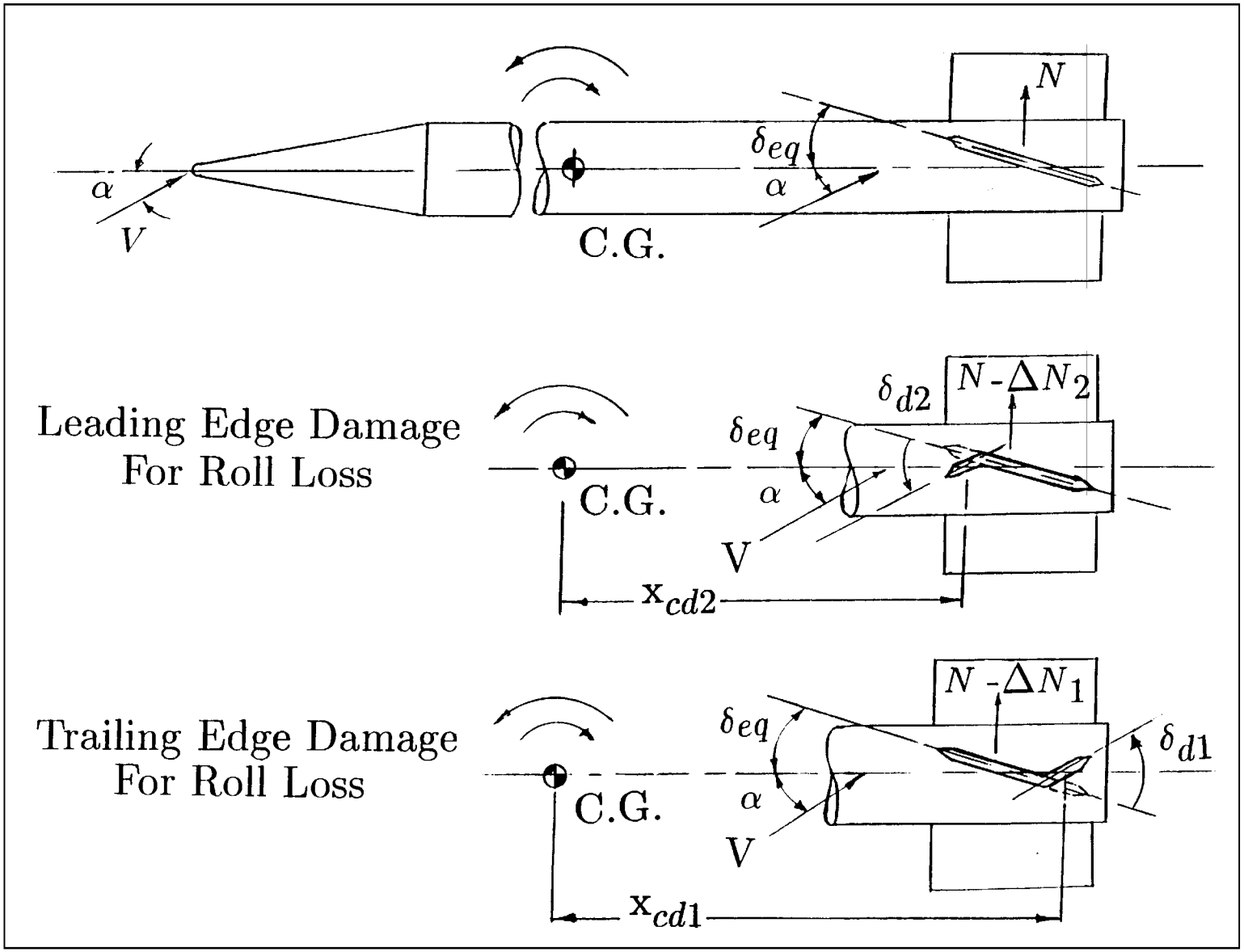

Figure 6. Leading and Trailing Edge Idealized Fin Damage.

cause a change in fin normal force and roll moment for an equivalent fin panel canted at δ_{eq}. The projectile roll is positive when clockwise (looking forward from the tail), and δ_{eq} is positive when it is up in the direction of producing positive roll. The static (non-rolling) asymmetries ΔC_N and ΔC_M (C_{Mo}) can be positive or negative, depending on the damage location and direction. Further details are discussed in the case study section.

2.4.4 *Mass Offset*

The projectile radial mass asymmetry is represented by the mass offset radial distance, Δcg. This offset, which always exists in real life with different degrees of severity, creates a rolling moment because of the normal force that acts on the aerodynamic, not the mass-center point of the rod cross section. This offset also gives rise to pitching and yawing moments attributable to the aerodynamic axial force (C_A), as can be seen in Figure 5 and reflected in Equations (5) and (6). An axial mass shift (i.e., shift along the body axis) was not considered explicitly as an asymmetry moment in this work. However, it can be considered as part of the off-design asymmetry moment, M_o, used here and which has primarily focused on moments resulting from fin damage.

A value of Δcg = 0.20d is extremely large and has been used only as an application example. Actual practical values are of the order of 0.003d to 0.009d for projectile applications. For missile applications, this offset is usually larger than those given for projectiles.

3. CASE STUDY

Calculations were performed to simulate the case of a subcaliber projectile that has a length/diameter (L/d) of 22.72, as given in Figure 2. The aerodynamic coefficients were obtained from the U.S. Army Research Laboratory (ARL) enclosed transonic range test database. In the enclosed range, the tests are made on steel models rather than on the actual design rounds for safety considerations. Therefore, simulations were also made for that particular case. The relevant information regarding this configuration is given in Table 1.

Table 1. Physical Properties of the Projectile

Ref. diameter	=	1.06 in.	(25.05 mm)
L/d	=	22.72	--
Material	=	steel	--
Mass	=	4.281 lb	(1.946 kg)
I_x	=	0.6956 lb-in^2	(2.04×10^{-4} kg-m^2)
I_y	=	143.56 lb-in^2	(0.42×10^{-1} kg-m^2)
Launch speed	=	5905.8 ft/s	(1806 m/s)
Launch spin	=	0 Hz	--

Twenty-three cases with four different steady state spin values were computed, covering the spectra of above/at/below the pitching frequency case. The pitching frequency was 25 Hz at launch (M = 5) and dropped to 23 Hz at Mach = 4.0 (or about t = 0.9 s). The different steady state spin cases were considered to reflect the effect of damaged fins. The actual equivalent fin cant angle for the projectile is estimated[15] to be 0.55°, resulting in a steady state spin of 90 Hz. Table 2 provides the fin cant angle values applied to simulate damaged fins and the corresponding steady state spin values. These chosen spin values were selected so as to provide insight about resonance behavior near and through the pitching frequency, ω_p.

Table 2. Equivalent Fin Cant and Steady State Spin

Case No.	Fin Status	Equiv. Fin Cant Angle, (deg)	Cant Angle as Fraction of δ_d	Steady State Spin (Hz)
I	undamaged	0.55	(1.0 δ_d)	90
IIa	damaged	0.22	(0.4 δ_d)	36
IIb	damaged (spin above ω_p)	0.165	(0.3 δ_d)	27
III	damaged (spin at ω_p)	0.137	(0.25 δ_d)	22.5
IV	damaged (spin below ω_p)	0.11	(0.2 δ_d)	18

For quantified fin damage, three idealized types were modeled, reflecting leading, trailing, and tip edge damage, as shown in Figure 7 for the six-fin configuration. The actual fin shown in Figure 8 is modeled by an equivalent fin panel wholly canted at $\delta_{eq} = 0.55^{\circ}$. Representative fin damage surface areas for the three types are also shown in the same figure. The corresponding change in fin normal force, ΔC_N, and ΔC_M were computed and are presented in Table 3. An idealized equivalent uniform fin cant angle damage for the six fins is listed. A single panel with a damaged area equivalent bend angle is modeled to provide the same lower spin rate that the six damaged fins would have. The corresponding change in the fin normal force, ΔC_N, and the corresponding change in C_M (i.e., C_{Mo}) were then computed. The corresponding values for damage Types I, II, and III are all listed in Table 3. The $C_{N\alpha}$ of the fin set, including its body interference effect, was computed by using the Naval Surface Warfare Center aerodynamic prediction (NSWC-AP95) fast design code[16]. Linear aerodynamics were used to provide engineering estimates for the fin damage angles in association with the damaged fin panel areas. For example, a 5% area fin damage bent at 8° would be equivalent to a 10% fin area damage bent at 40°. This is based on the relation that a fin panel lift is linearly proportional to the product of its surface area and the surface angle of attack. Although this linearity may not be valid for large angles, it simplifies the procedure. More sophisticated nonlinear models may obviously be devised.

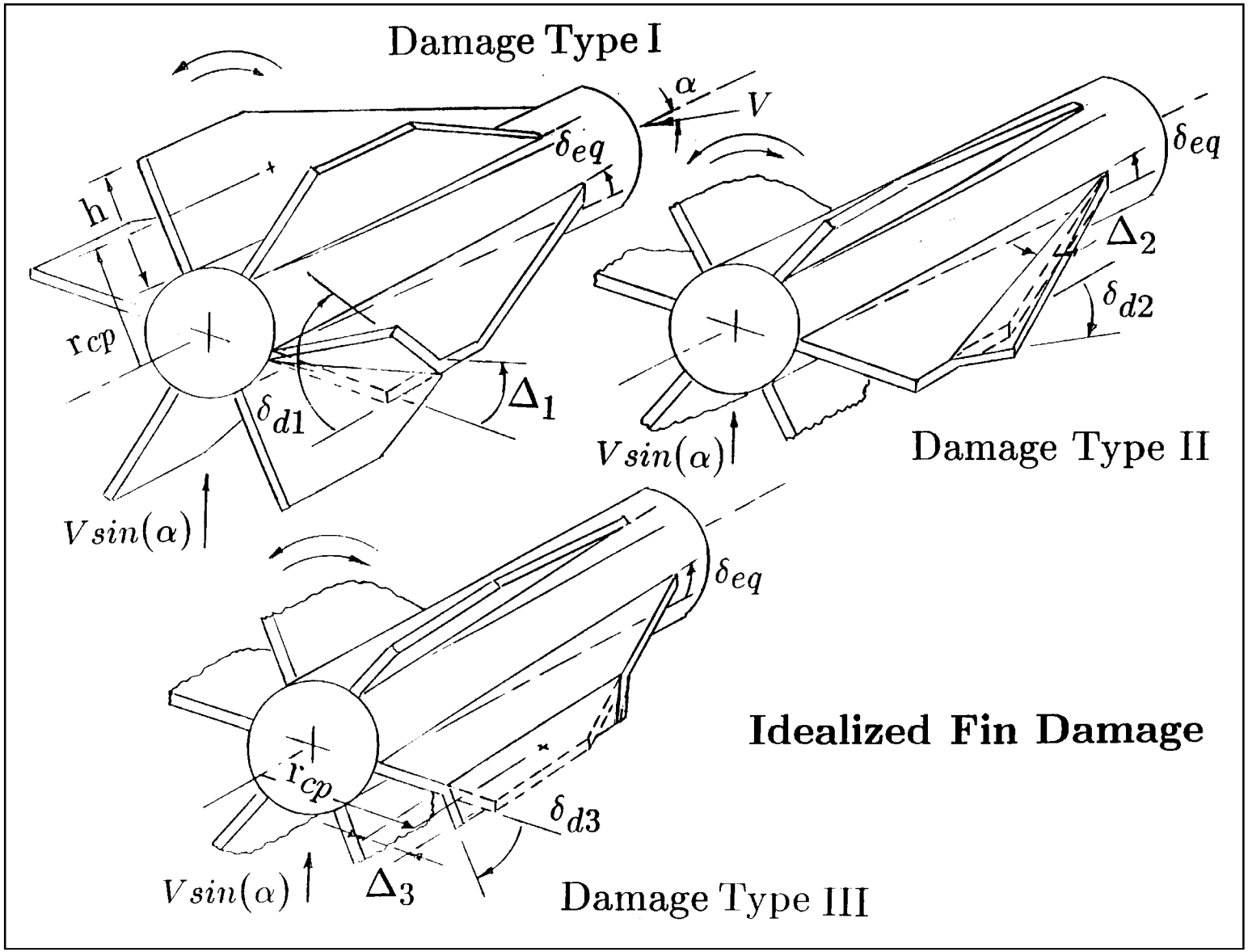

Figure 7. Three Types of Idealized Fin Damage.

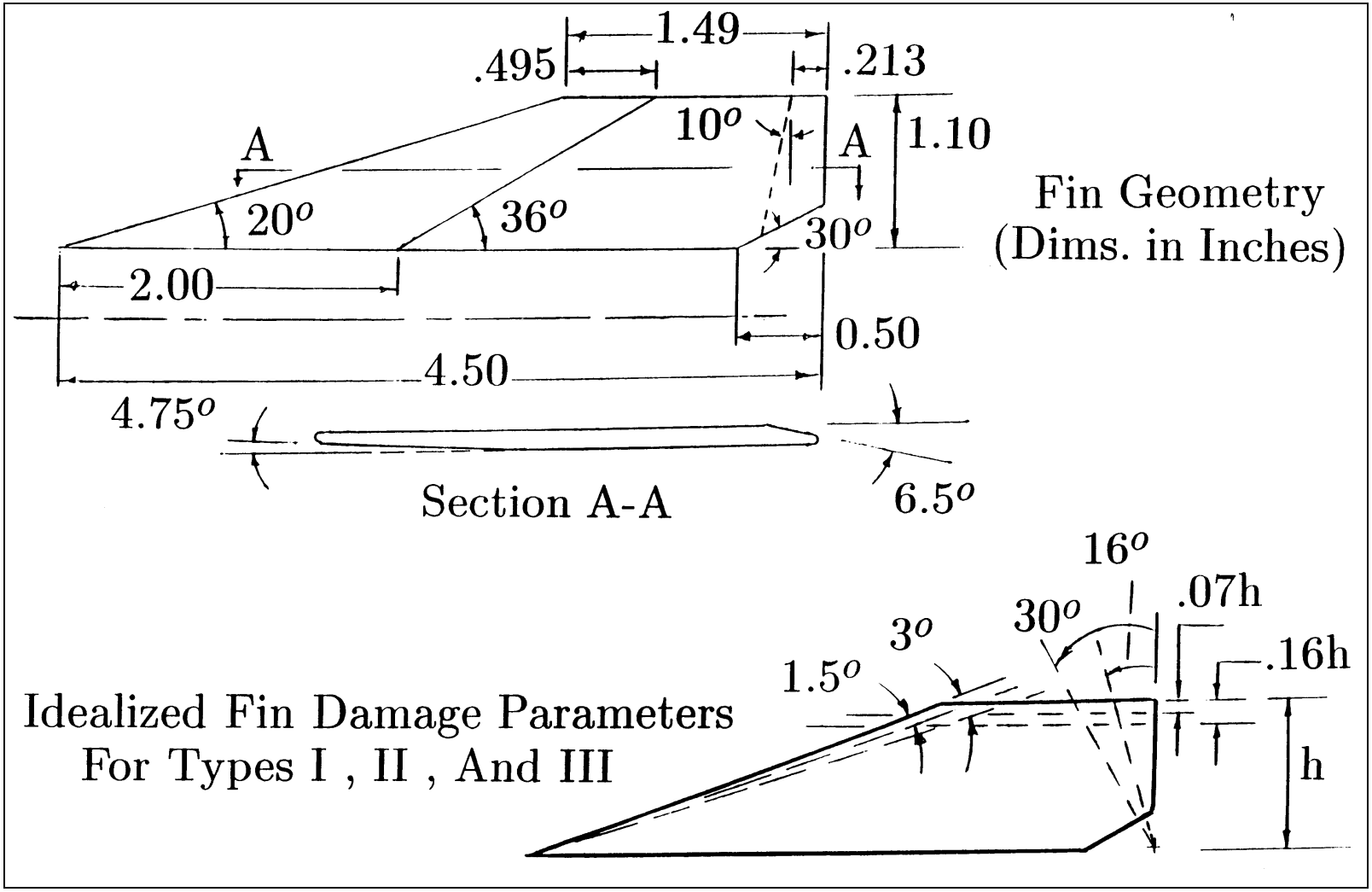

Figure 8. Quantified Fin Area Damage for Types I, II, and III.

Table 3. Damaged Fin Areas and Angles With Their Corresponding ΔC_N and ΔC_M

Resulting Reduced Roll Rate (Hz)	Uniform Damage to Six Fins			Equivalent Damage to a Single Fin			Single Fin Damage Parameters and Forces								
							Damage Type I		Damage Type II		Damage Type III				
	Initial δ_{eq} (deg)	δ_{dg} (deg)	Final δ_{eq} (deg)	δ_{dg}, whole panel (deg)	Damaged Area (Ad/Af)	δ_{dg} (deg)	Δ1 (deg)	δ1 (deg)	Δ2 (deg)	δ2 (deg)	Δ3 (in)	δ3 (deg)	ΔC_N ($\equiv C_{No}$)	ΔC_M ($\equiv C_{Mo}$) Damage Type I	II	III
36	0.55	−0.33	0.22	−1.43	0.05	−28.6	16	+28.6	1.5	−28.6	0.07h	28.6	−0.094	+0.97	+0.78	+0.93
					0.10	−14.3	30	+14.3	3.0	−14.3	0.16h	14.3				
27	0.55	−0.385	0.165	−1.76	0.05	−35.2	16	+35.2	1.5	−35.2	0.07h	−35.2	−0.116	+1.20	+0.96	+1.15
					0.10	−17.6	30	+17.6	3.0	−17.6	0.16h	−17.6				
22.5	0.55	−0.412	0.138	−1.92	0.05	−38.4	16	+38.4	1.5	−38.4	0.07h	−38.4	−0.126	+1.31	+1.04	+1.25
					0.10	−19.2	30	+19.2	3.0	−19.2	0.16h	−19.2				
18	0.55	−0.44	0.11	−2.09	0.05	−41.8	16	+41.8	1.5	−41.8	0.07h	−41.8	−0.137	+1.42	+1.14	+1.36
					0.10	−20.9	30	+20.9	3.0	−20.9	0.16h	−20.9				

Different independent values for the mass offset were used, ranging between 0.0d and 0.20d. $C_{M\alpha}$, for the undamaged projectile was -35 at the launch speed. Values for C_{Mo} varying between 0.0 and +2.444 (corresponding to 0.0° and -4.0° static trim angle) were used. The numerical values used for both parameters are listed separately in Table 4.

Table 4. List for the Independent Values Used for Mass Offset and Asymmetry Moment

Mass Offset, Δcg/d	C_{Mo}	The Corresponding Trim Angle for C_{Mo} (deg)
0.0	0.0	0.0
0.001	+0.061	-0.1
0.004	+0.122	-0.2
0.01	+0.305	-0.5
0.04	+0.428	-0.7
0.08	+0.489	-0.8
0.10	+0.916	-1.5
0.12	+1.222	-2.0
0.20	+2.444	-4.0

4. COMPUTATIONS

Computations were made by solving the three equations as an initial value problem. The alpha and beta equations were solved simultaneously, then followed by the roll equation. Small time steps were used ($\Delta t = 3.0 \times 10^{-6}$ s). Three-point, central differences, second order accurate (in time) finite differencing was used, with recurrence relations relating the variable value at the n+1 time level to the previous n and n-1 time levels. Knowing the first two values at time zero and at Δt using the initial conditions, one can then proceed directly.

The roll equation was solved as a first order equation in $\dot{\phi}$, with the boundary condition given by Equation (4). Equation (2) was written as

$$I_x \left(\dot{\phi}\right)_n + BB\big|_n \; \dot{\phi}_n + CC\big|_n = 0 \tag{8}$$

The solution was then computed as

$$\dot{\phi}_{n+1} = \dot{\phi}_n - \Delta t \left[BB\big|_n \; \dot{\phi}_n + CC\big|_n \right] / I_x \tag{9}$$

The roll equation is coupled to the pitch/yaw equations through the induced roll moment term which includes α_t and C_{li}.

Calculations were usually stopped at about t = 0.9 s, which corresponds, for the case considered, to a distance of about 5,578 ft (1700 m) down from the gun muzzle. This

corresponds to about 300,000 time steps. A single case takes about 15 seconds on a UNIX™ minicomputer (workstation).

5. RESULTS

Because of the many parameters of the problem, one set of similar conditions was applied so that the spin/pitch lock-in phenomenon can be observed without changing the parameters. Later studies may be made with these parameters as variables to discuss their individual influences in detail.

The initial conditions were, for example, held the same for all cases. The values $\alpha(t_o) = 4^\circ$; $\beta(t_o) = 3^\circ$; $\dot{\alpha}(t_o) = 1.0$ rad/s; and $\dot{\beta}(t_o) = 1.0$ rad/s were used.[17] The roll equation was also solved under zero initial values for both ϕ and $\dot{\phi}$. Any other values may obviously be prescribed for other desired conditions. Relatively large values for the initial yaw angles ($\alpha = 4^\circ$ and $\beta = 3^\circ$) were used to illustrate the point that these angles will quickly dampen to small values close to zero in no-lock-in cases. This usually occurs after less than 0.6 second, or about 800 meters from the the muzzle, for the present configuration.

Other parameters are the mass offset initial location angle, Γ, and the C_{Mo} moment orientation angle, λ. They were taken to be 30° and 70°, respectively. Reference 4 provides a discussion about λ angle role in the lock-in. A list of cases computed in this study, including the corresponding values of the parameters used, is provided in the form of Table 5.

First, the case of spinning above ω_p with steady state spin of 36 Hz is presented. This case Number 1, with no fin damage or asymmetries was computed and the typical α- and β-angle histories are given in Figure 9, both approaching zero values at about t = 0.6 s.

Case Numbers 2 through 10 were computed with varying Δcg but with zero C_{Mo}. For the higher spin rate of 36 and 27 Hz, no lock-in occurred with the given values of Δcg, as shown in Figures 10 and 11, respectively. Although the value 0.20d is relatively large and is not expected in practice, one must remember that no C_{Mo} was applied here, which is not the case in real life. However, as the steady state spin caused by damage gets closer to the pitch frequency, such as for the cases of 22.5 and 18 Hz, lock-in occurs with a smaller value of Δcg. Figure 12 indicates the lock-in for the 18-Hz case after about 0.5 s from launch.

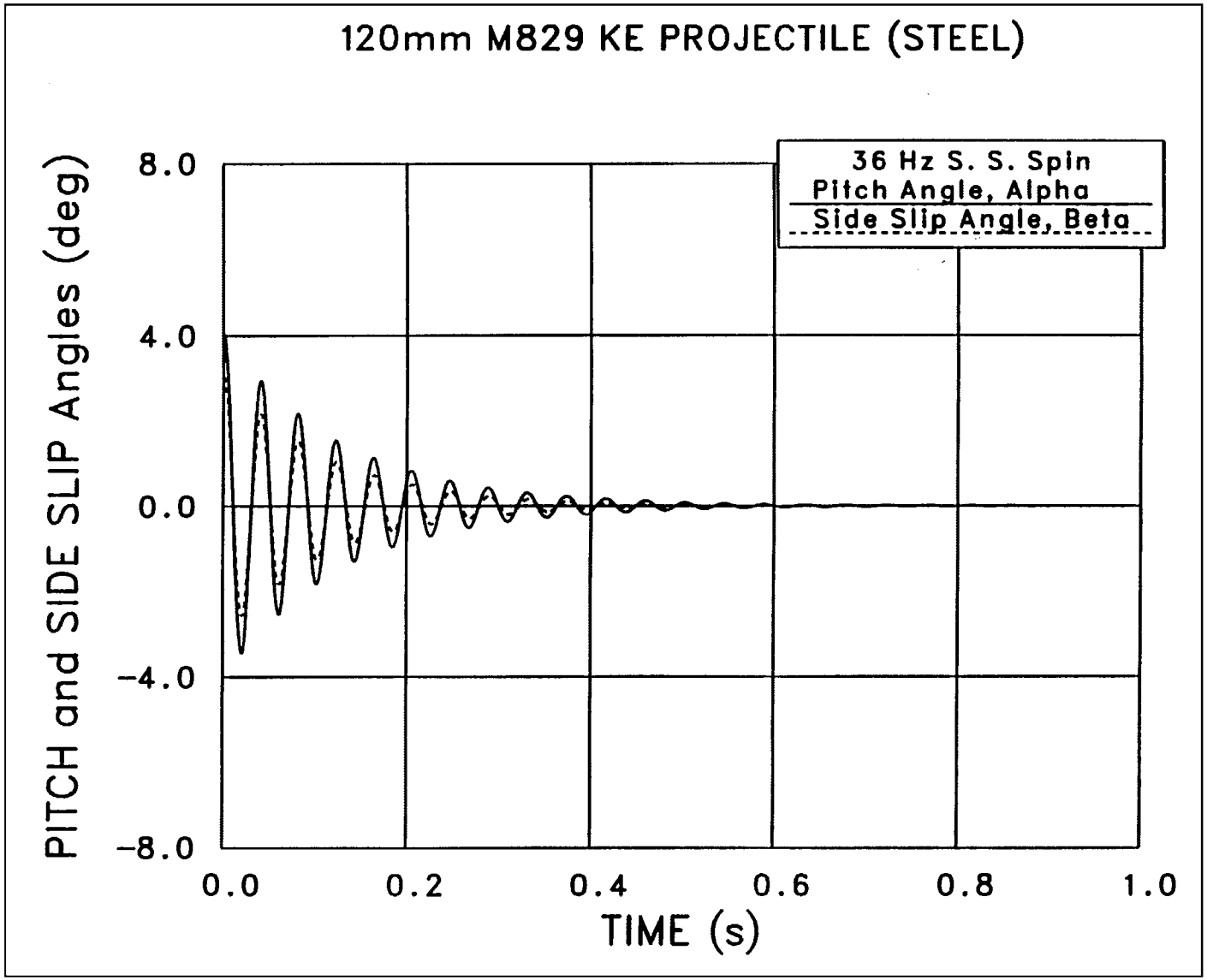

Figure 9. Pitch and Side Slip Angles for No-Lock-in Case ($\delta_{eq} = 0.4\ \delta_d$, $C_{Mo} = 0.0$, $\Delta cg = 0.0$) .

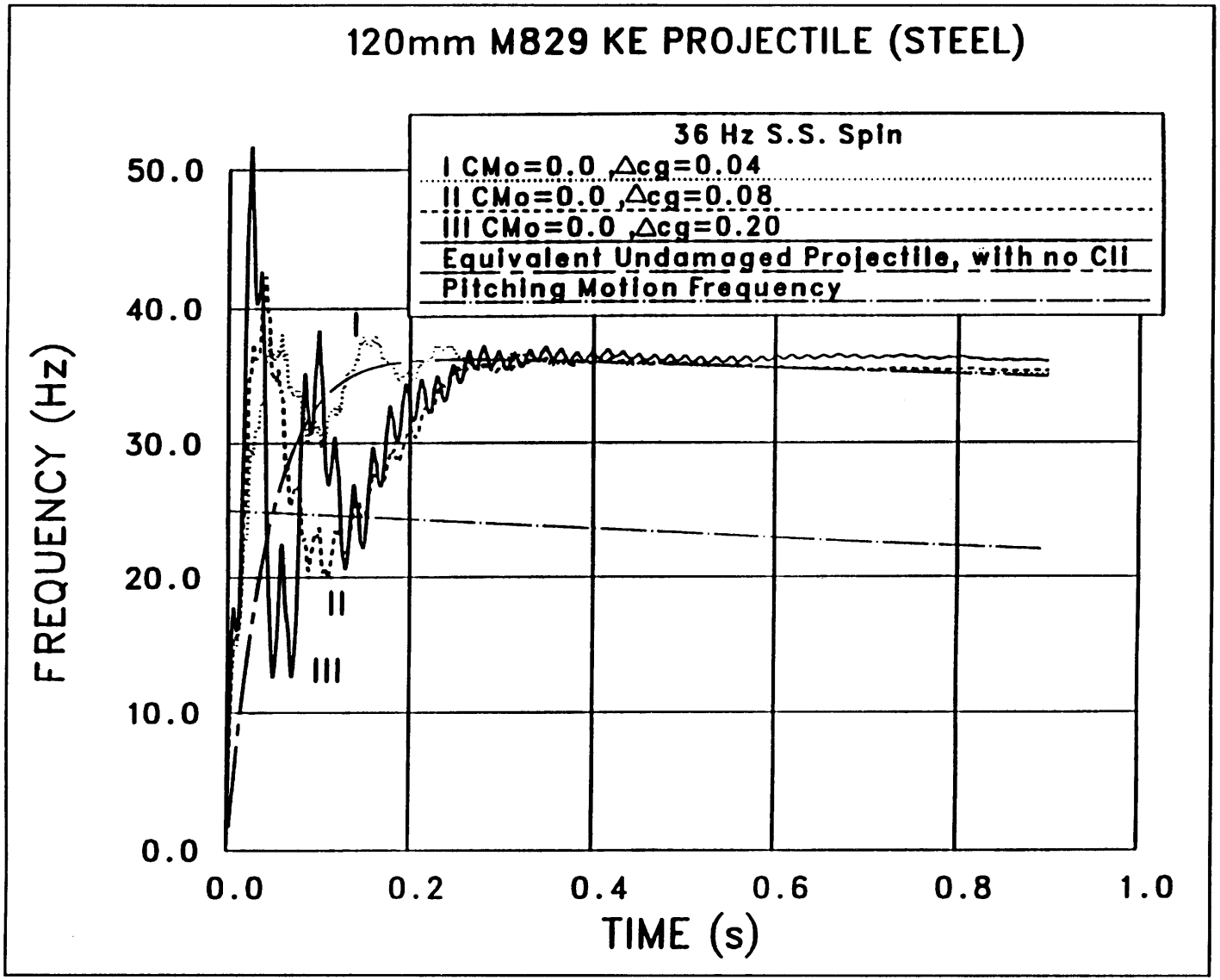

Figure 10. Roll/pitch Resonance and Then Escaping Pitch Lock-in ($\delta_{eq} = 0.4\ \delta_d$, $C_{Mo} = 0.0$, and increasing Δcg).

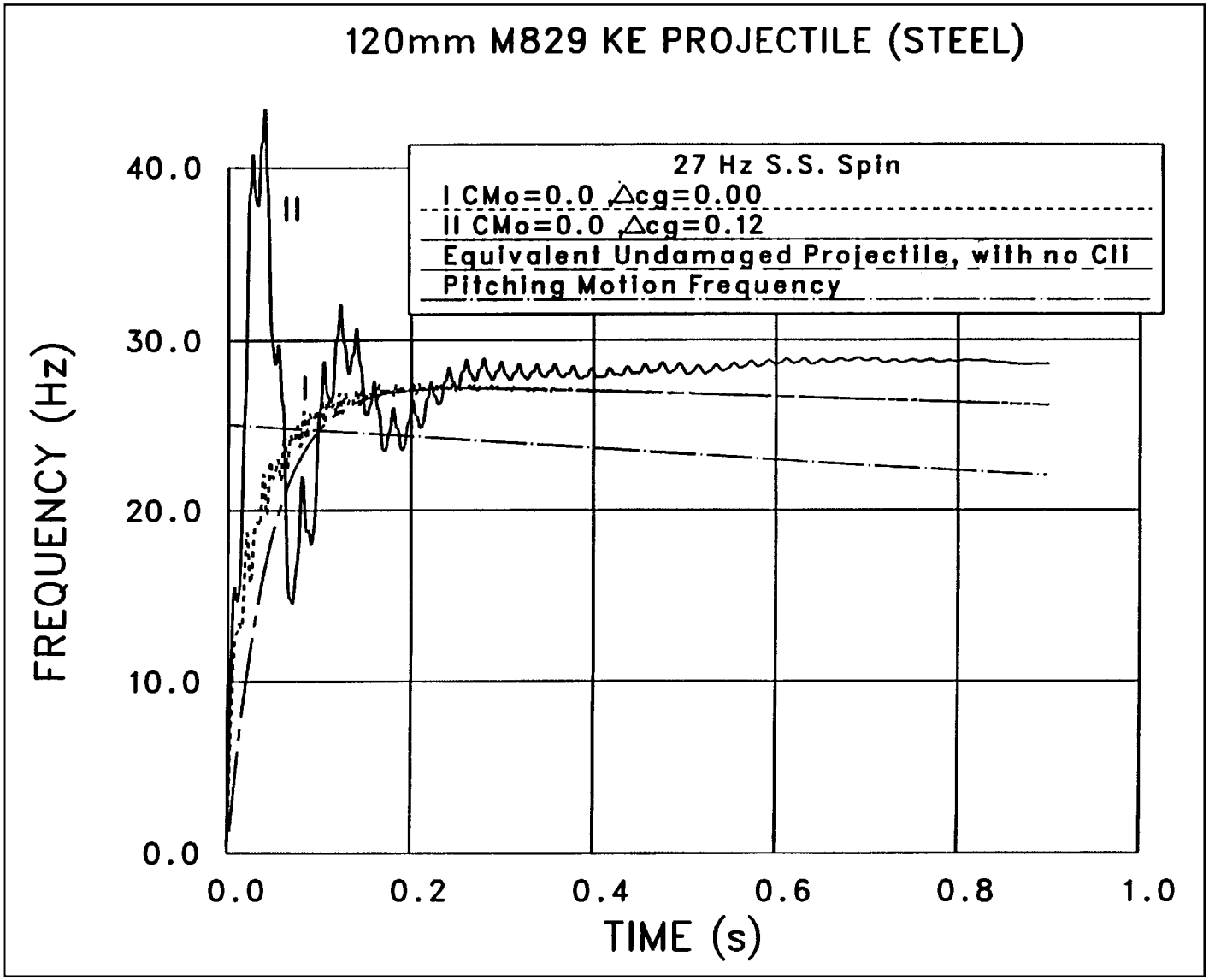

Figure 11. Roll/pitch Resonance and Then Escaping Pitch Lock-in ($\delta_{eq} = 0.3\ \delta_d$, $C_{Mo} = 0.0$, and increasing Δcg).

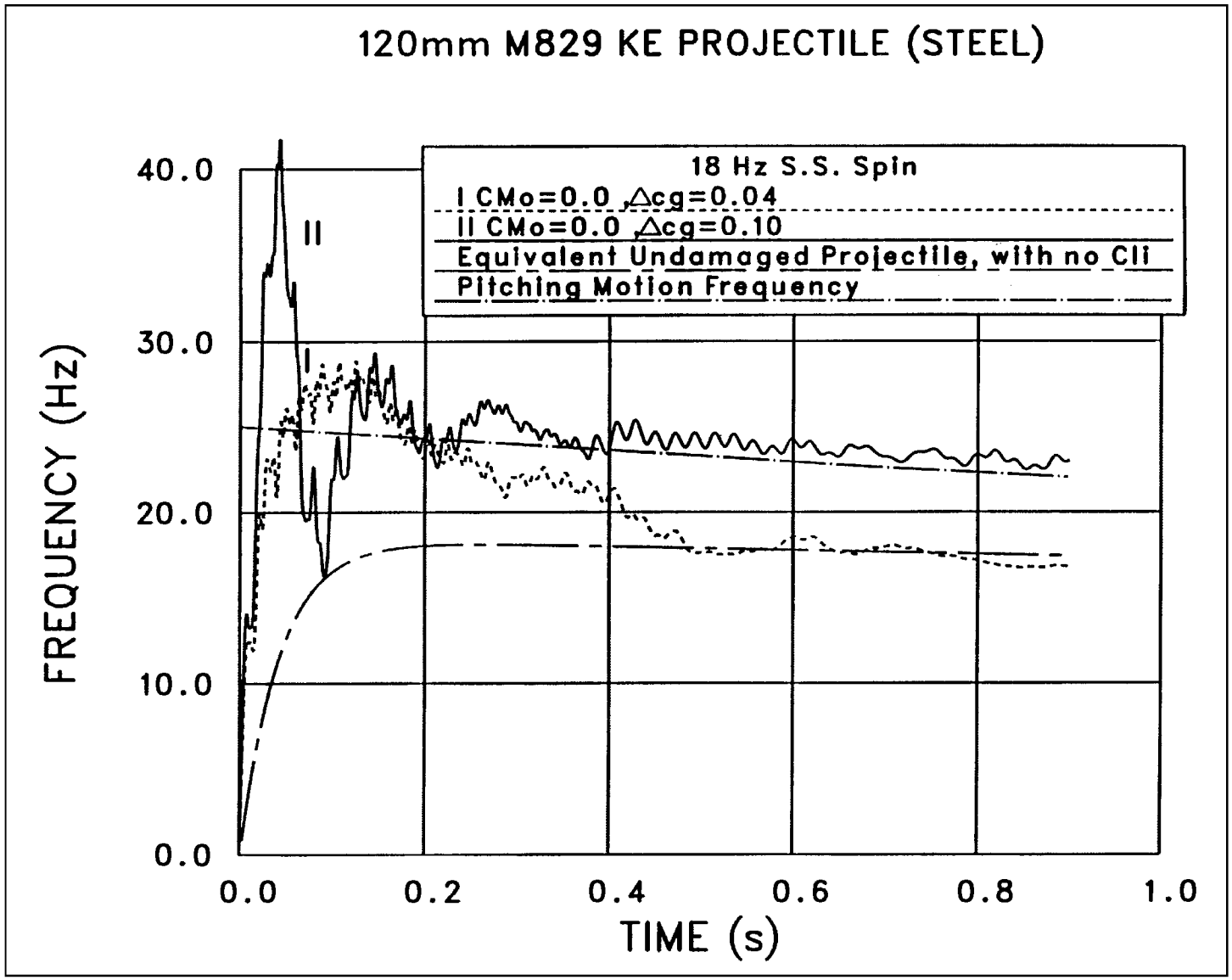

Figure 12. Roll/pitch Resonance and Roll/pitch Lock-in (δ_{eq} = 0.2 δ_d , C_{Mo} = 0.0, and increasing Δcg).

Table 5. Cases Computed and Parameter Values

Case No.	Equiv. Fin Cant Angle	C_{Mo}	C_{Mo} Correspond. Trim Angle (deg)	Δ cg/d	Lock-in Status
1	$0.4\,\delta_d$	0.0	0.0	0.04	no lock
2	$0.4\,\delta_d$	0.0	0.0	0.08	no lock
3	$0.4\,\delta_d$	0.0	0.0	0.20	no lock
4	$0.3\,\delta_d$	0.0	0.0	0.0	no lock
5	$0.3\,\delta_d$	0.0	0.0	0.04	no lock
6	$0.3\,\delta_d$	0.0	0.0	0.12	no lock
7	$0.25\,\delta_d$	0.0	0.0	0.0	no lock
8	$0.25\,\delta_d$	0.0	0.0	0.08	lock-in
9	$0.2\,\delta_d$	0.0	0.0	0.0	no lock
10	$0.2\,\delta_d$	0.0	0.0	0.10	lock-in
11	$0.4\,\delta_d$	+0.305	-0.5	0.0	lock-in
12	$0.4\,\delta_d$	+0.916	-1.5	0.0	lock-in
13	$0.4\,\delta_d$	+2.444	-4.0	0.0	lock-in
14	$0.3\,\delta_d$	0.0	0.0	0.0	no lock
15	$0.3\,\delta_d$	+0.428	-0.7	0.0	lock-in
16	$0.3\,\delta_d$	+1.222	-2.0	0.0	lock-in
17	$0.25\,\delta_d$	0.0	0.0	0.0	no lock
18	$0.25\,\delta_d$	+0.061	-0.2	0.0	lock-in
19	$0.2\,\delta_d$	0.0	0.0	0.0	no lock
20	$0.2\,\delta_d$	+0.610	-2.0	0.0	lock-in
21	$0.4\,\delta_d$	+0.061	-0.10	0.001	no lock
22	$0.4\,\delta_d$	+0.122	-0.20	0.040	no lock
23	$0.4\,\delta_d$	+0.489	-0.80	0.100	lock-in

Case Numbers 11 through 20 examine the effect of increasing the value of C_{Mo} without the mass offset influence being present. Figure 13 depicts the effect of increasing C_{Mo} for the fin damage spin of 36 Hz. It is interesting to note that for smaller fin damage, it takes longer to lock in, while for larger damage, lock-in occurs faster and with closer value to the pitch frequency. The same behavior is depicted in Figure 14 for the fin damage of 27-Hz steady state spin. Figure 15 depicts the yaw angle amplification factor for this later case. The amplification factor here is defined as the computed total angle of attack,

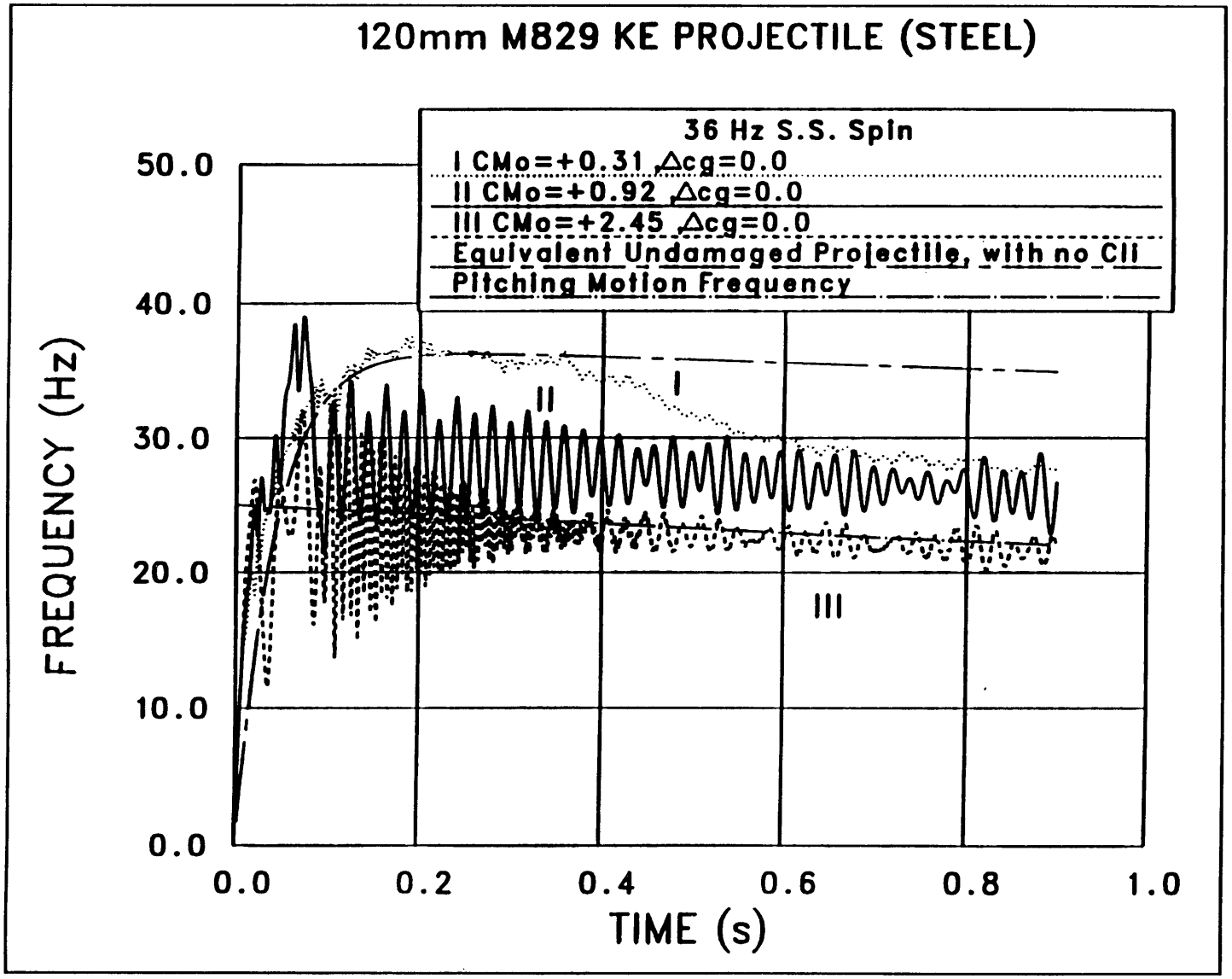

Figure 13. Roll/pitch Lock-in ($\delta_{eq} = 0.4\ \delta_d$, increasing C_{Mo} , $\Delta cg = 0.0$).

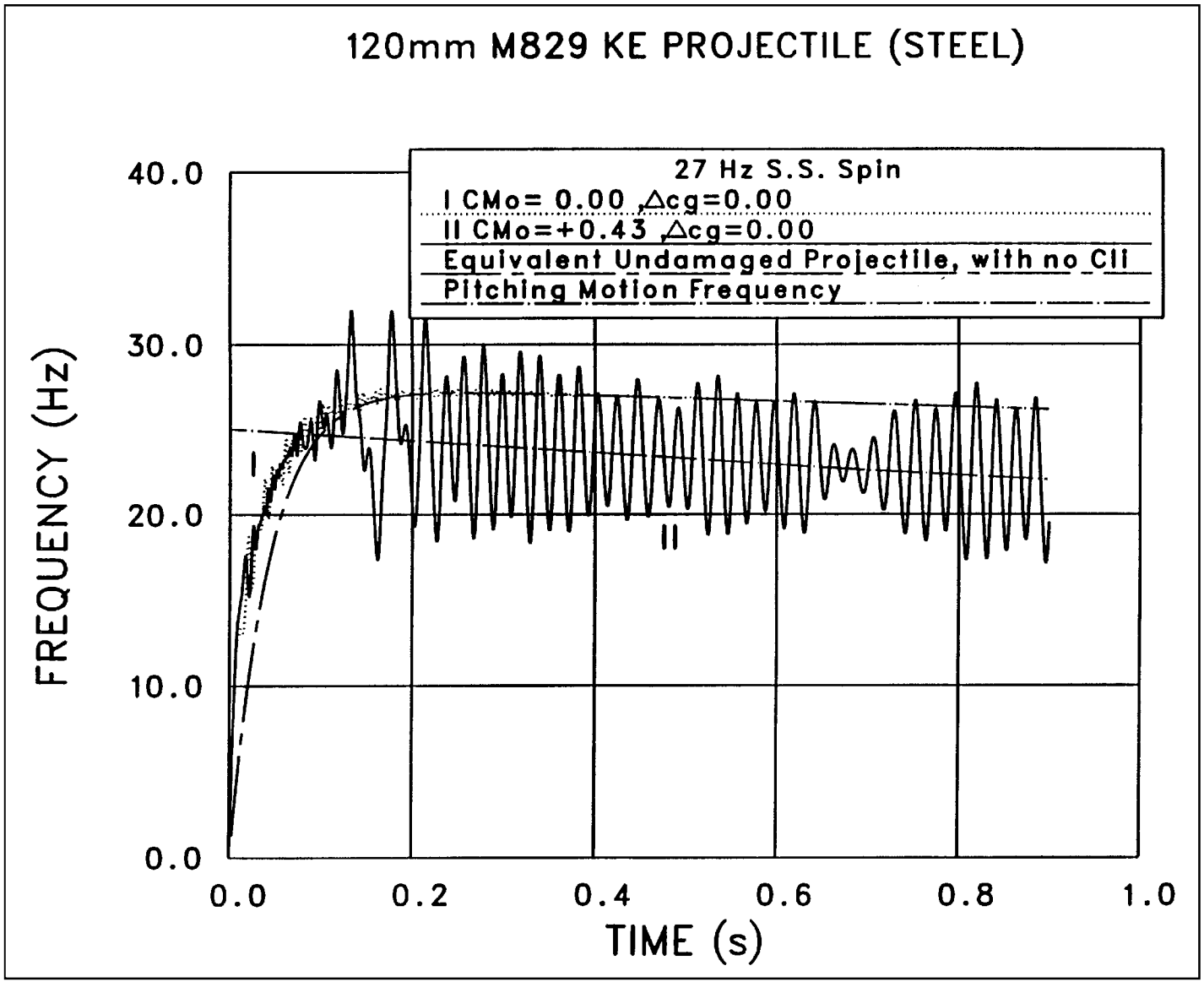

Figure 14. Roll/pitch Lock-in and No Lock-in ($\delta_{eq} = 0.4\ \delta_d$, increasing C_{Mo} , $\Delta cg = 0.0$).

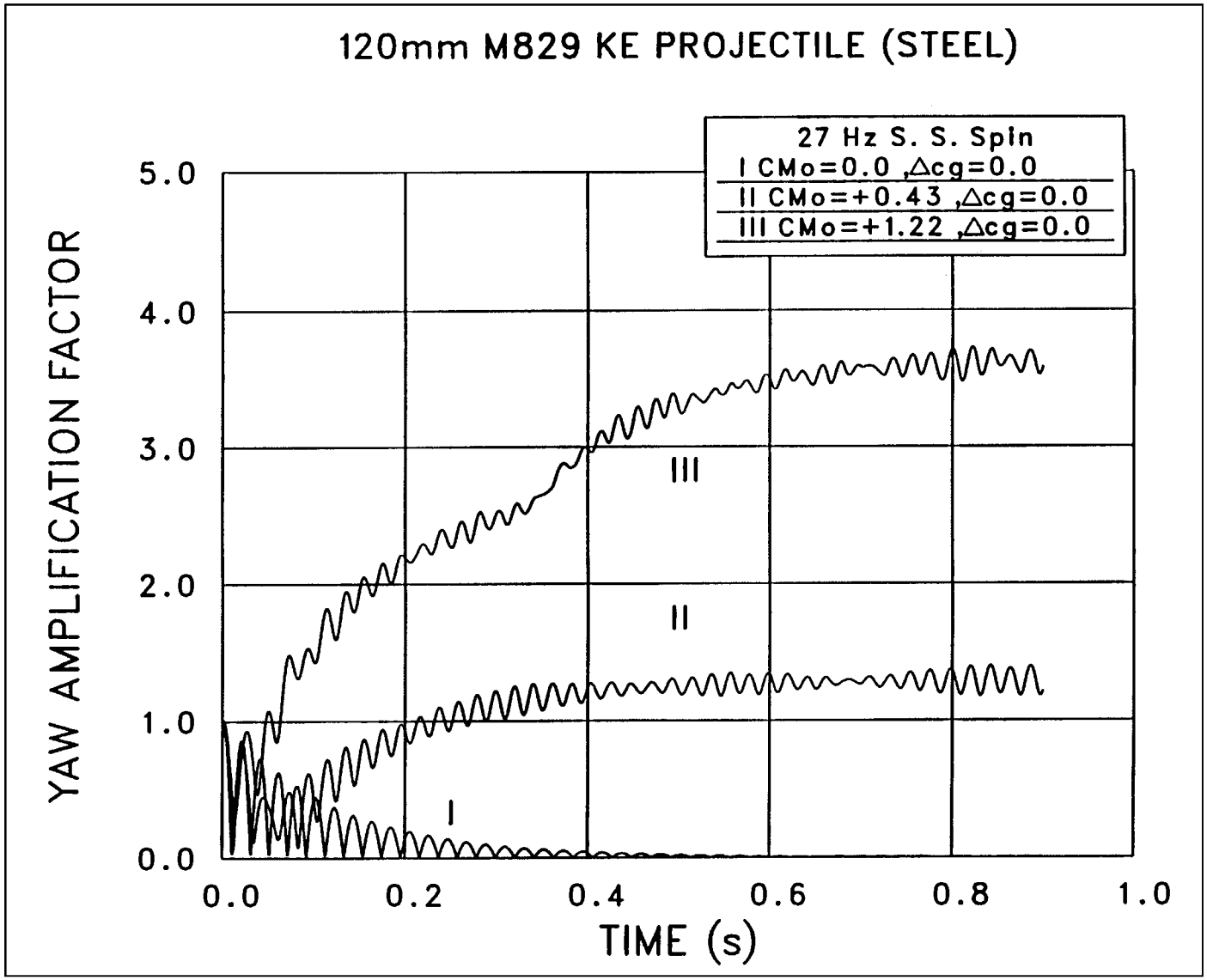

Figure 15. Yaw Angle Amplification for Roll/pitch Lock-in ($\delta_{eq} = 0.3\ \delta_d$, increasing C_{Mo} , $\Delta cg = 0.0$).

divided by the initial total angle of attack. Amplification factors of 1.2 and 3.6 are noticed for cases of lock-in with fin damage, while attenuation to a value of zero is noticed, as expected, for the case with no fin damage (no lock-in).

In real life, usually cases with both asymmetries and mass offset occur. Cases 21 through 23 were computed showing increased values for both C_{Mo} and Δcg. Pitch resonance changes to pitch lock-in when both parameters were increased as reflected by Case Numbers 21 through 23 of Table 5 and shown in Figure 16. Figure 16 also shows the change from short-lived pitch resonance to full lock-in with ω_p when the asymmetry damage increased. Figure 17 shows the α- and β-angle histories for Case Number 21, which reflects very small asymmetries. The plot indicates almost unaffected motion.

The expected impact imprint on cardboard yaw cards (or wire mesh screens) used in measuring the "yaw" motion in practical ballistics can now be constructed from the results computed. Figure 18 presents the α- and β-angle histories for Case Number 12 for lock-in. Figure 19 depicts the expected imprint for the lock-in case of Figure 18 at t = 0.633 s, in which $|\alpha|$ and $|\beta|$ were computed to be 3.54° and 1.28°, respectively, with a total yaw angle of 3.76°. A harsher case of lock-in with a larger C_{Mo} is reflected in Figures 20 and 21. The $|\alpha|$ and $|\beta|$ computed were 9.44° and 5.60°, respectively, thus yielding a total yaw angle of 11.97° at t = 0.194 s.

In the practice of ballistics, the $\alpha - \beta$ plot is usually monitored to provide insight into the flight. The three cases of no lock-in, late lock-in, and immediate lock-in are presented in Figures 22 through 24. Figure 22 provides the typical KE flight pattern with no asymmetry and therefore, no lock-in. Figure 23 shows Case Number 11 which locked in later in its flight, as was also indicated by Curve Number 1 of Figure 13. Figure 24 depicts the case of a quick roll/pitch lock-in of Case Number 23. All cases started, as can be seen, with the same initial conditions of $\alpha = 3^\circ$ and $\beta = 4^\circ$.

Additional cases can now be routinely computed. Reference 4 provides a simple "guideline" for the expected values for both asymmetry parameters for lock-in. These values may be used as first estimate for the value of the parameter under which the vehicle may lock in. The exact value can then be determined by computing the case with perturbations on these estimates and monitoring the resulting spin history, and the $\alpha - \beta$ plot.

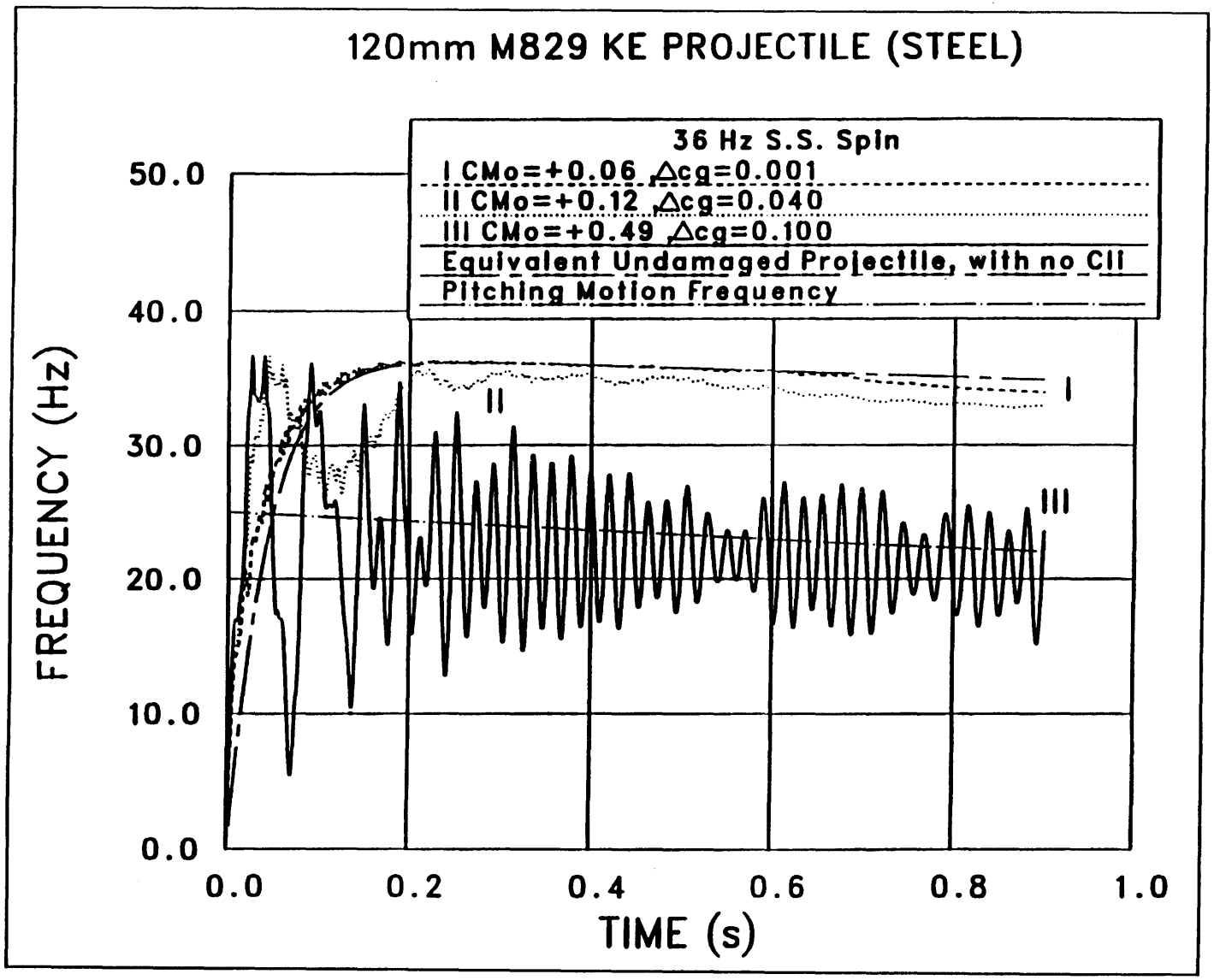

Figure 16. Roll Resonance and Roll/pitch Lock-in ($\delta_{eq} = 0.4\ \delta_d$ and increasing C_{Mo} and Δcg).

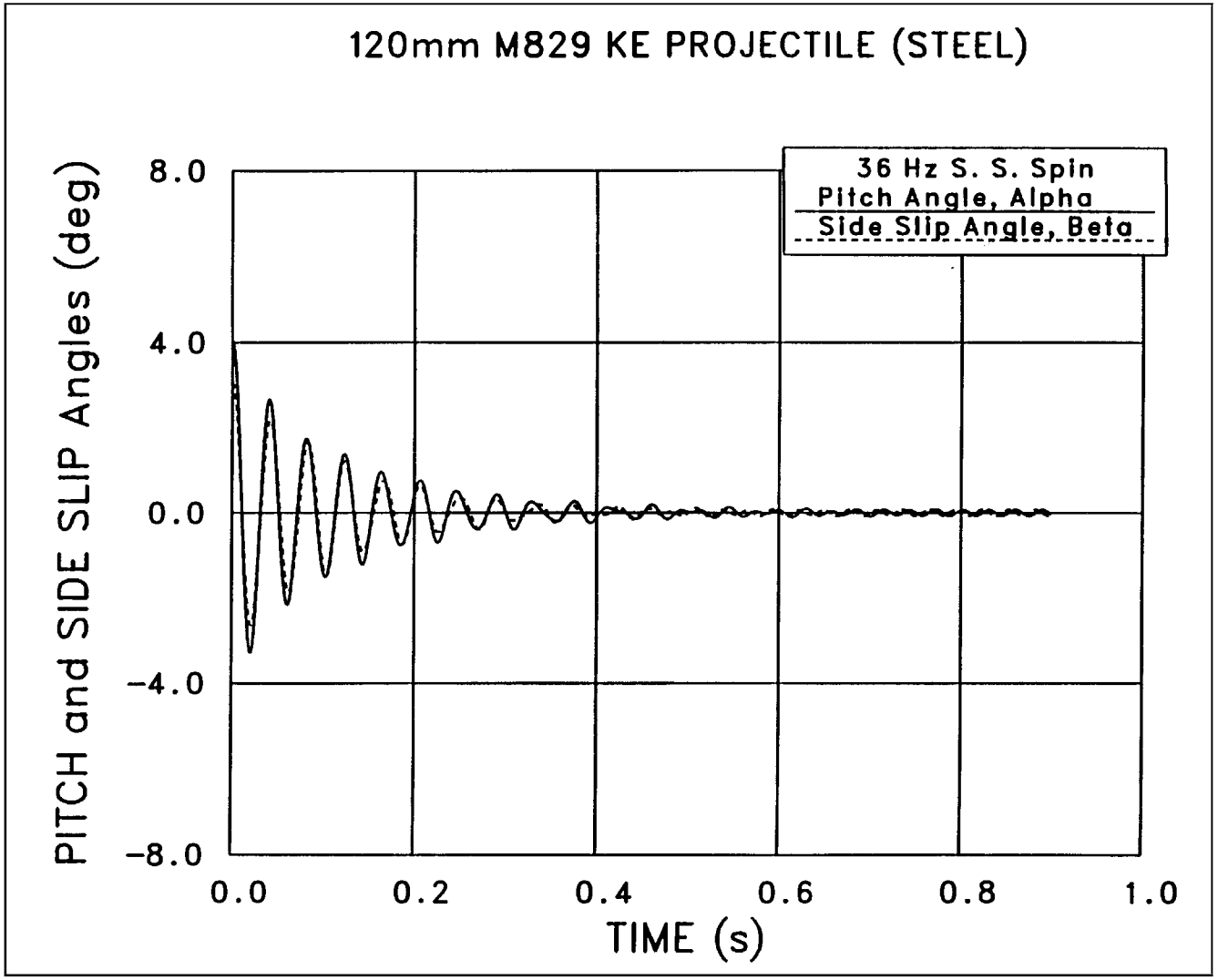

Figure 17. Pitch and Side Slip Angles for a Case of Very Slight Asymmetries ($\delta_{eq} = 0.4\ \delta_d$, $C_{Mo} = +0.061$, and $\Delta cg = 0.001$).

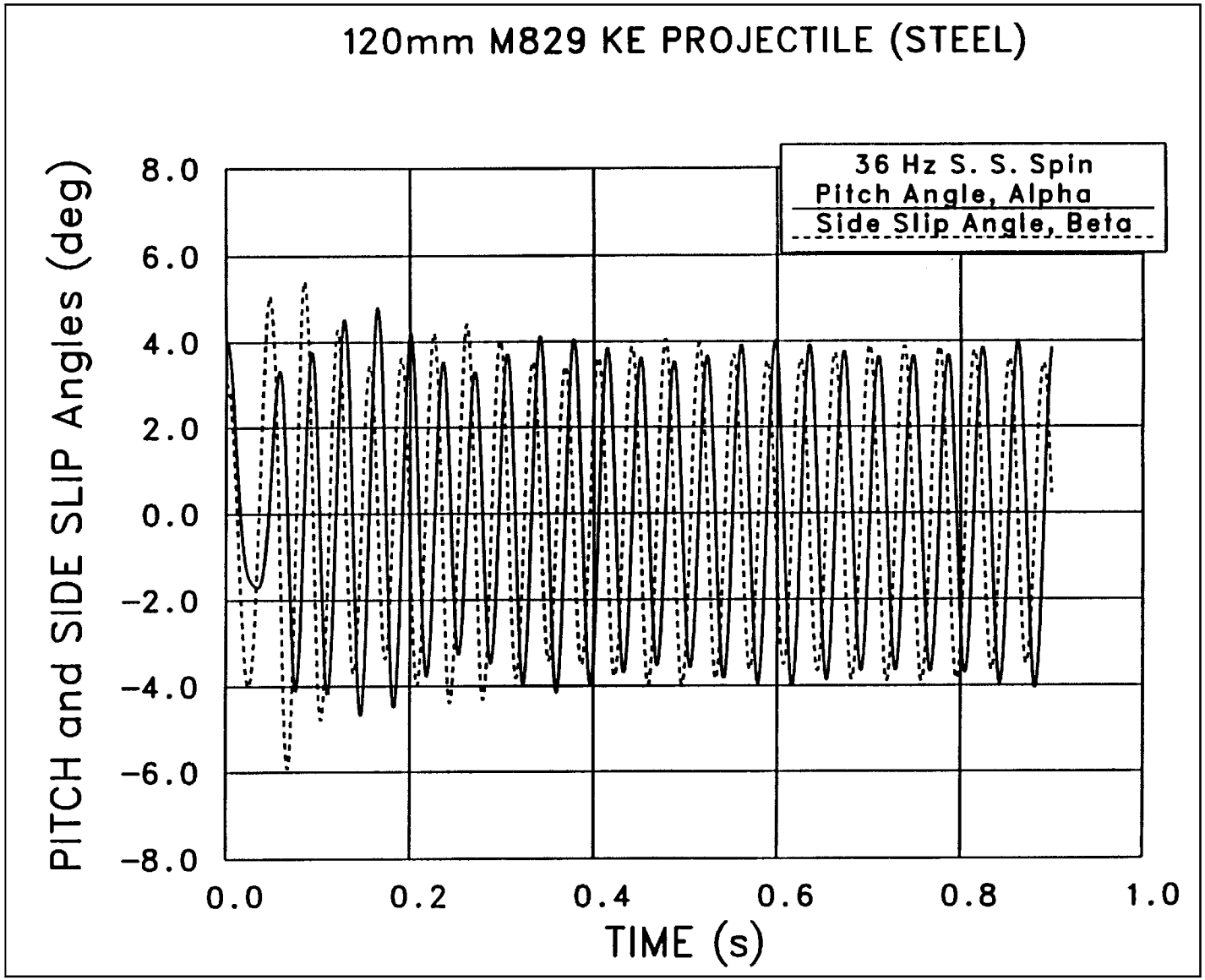

Figure 18. Pitch and Side Slip Angles for a Case of Roll/pitch Lock-in ($\delta_{eq} = 0.4\ \delta_d$, C_{Mo} = +2.444, and Δcg = 0.0).

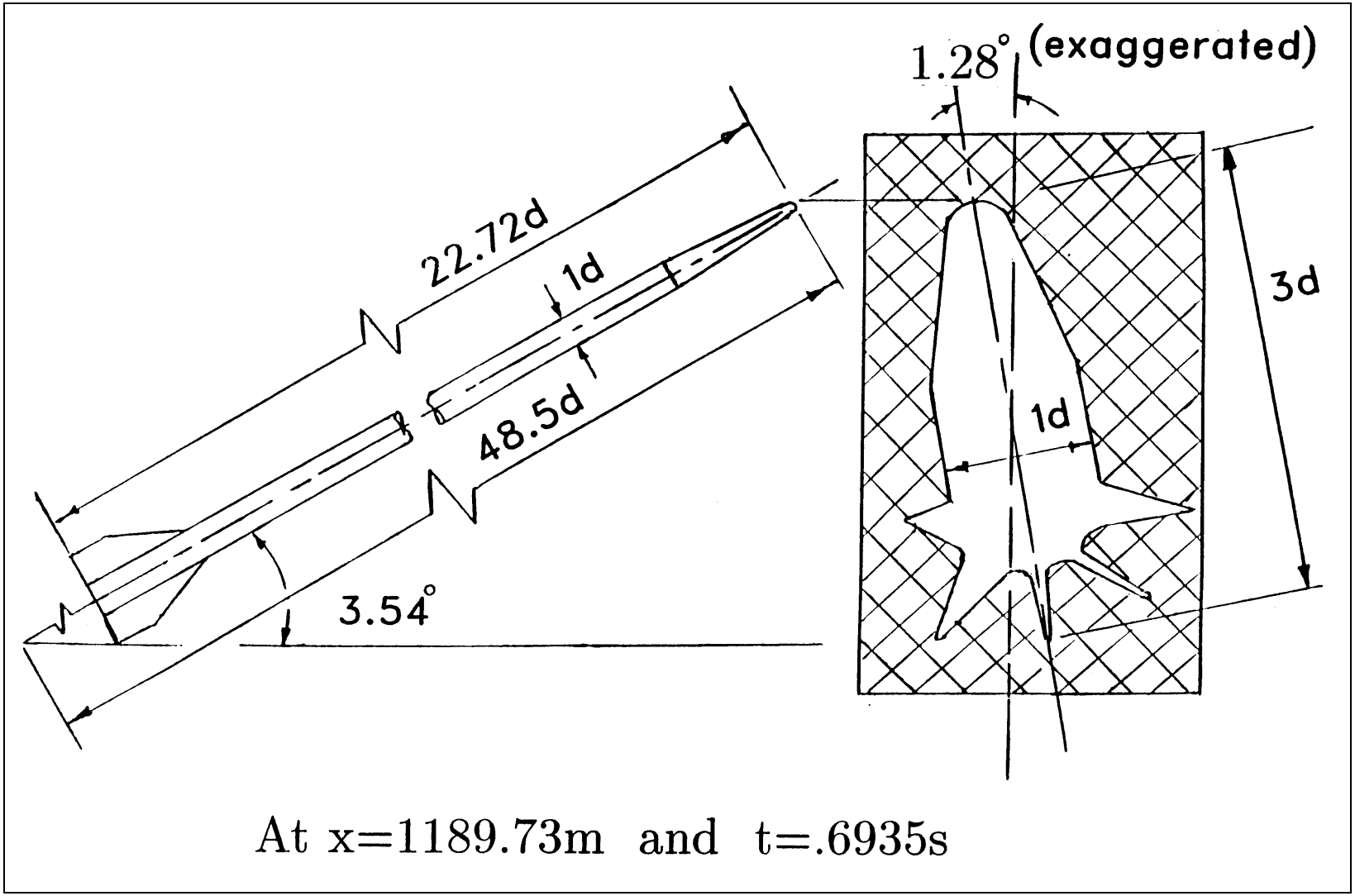

Figure 19. Predicted Impact Imprint of a Case of Roll/pitch Lock-in ($\delta_{eq} = 0.4\ \delta_d$, C_{Mo} = +0.916, and Δcg = 0.0).

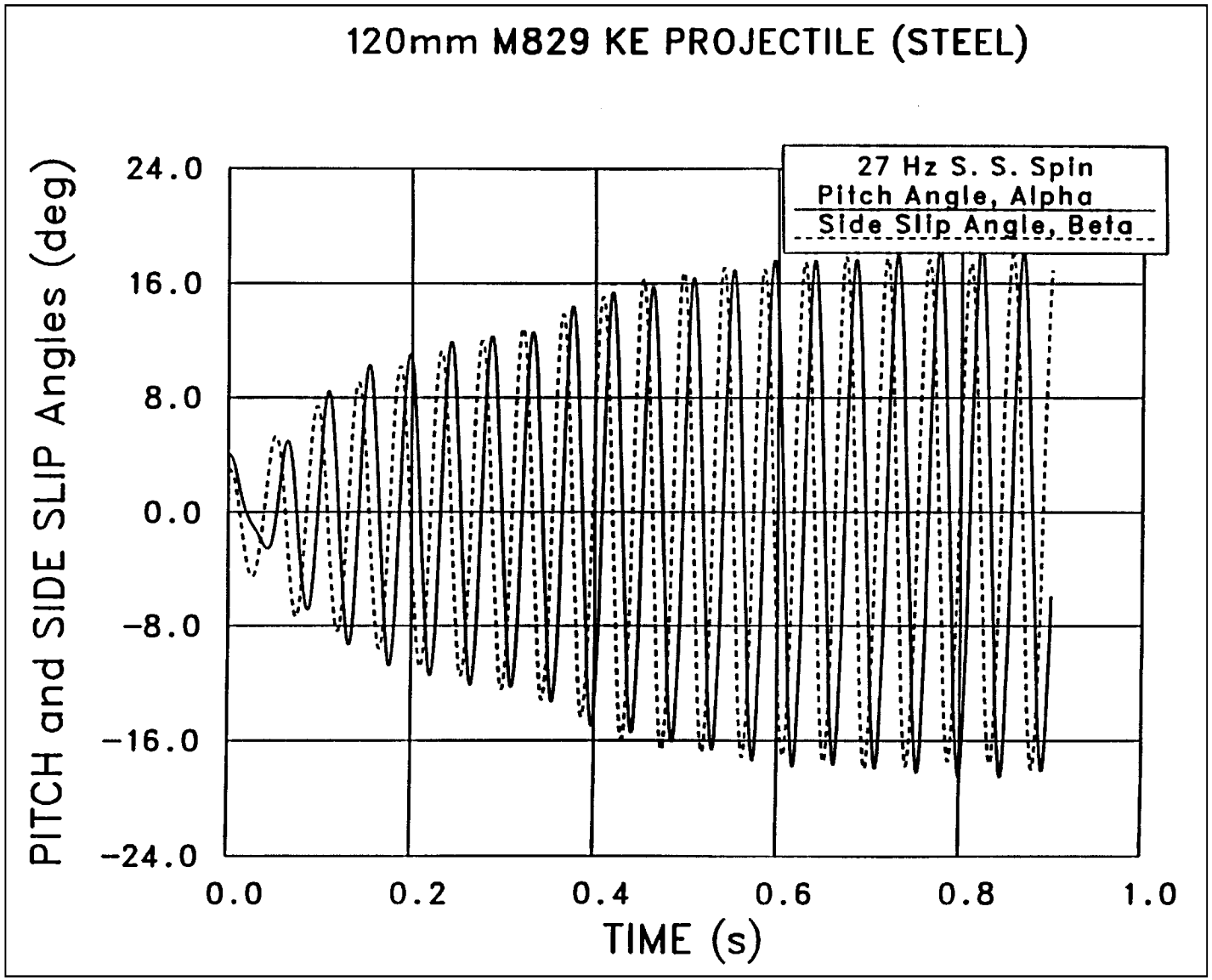

Figure 20. Pitch and Side Slip Angles for a Case of Roll/pitch Lock-in ($\delta_{eq} = 0.3\ \delta_d$, C_{Mo} = +1.222, and Δcg = 0.0).

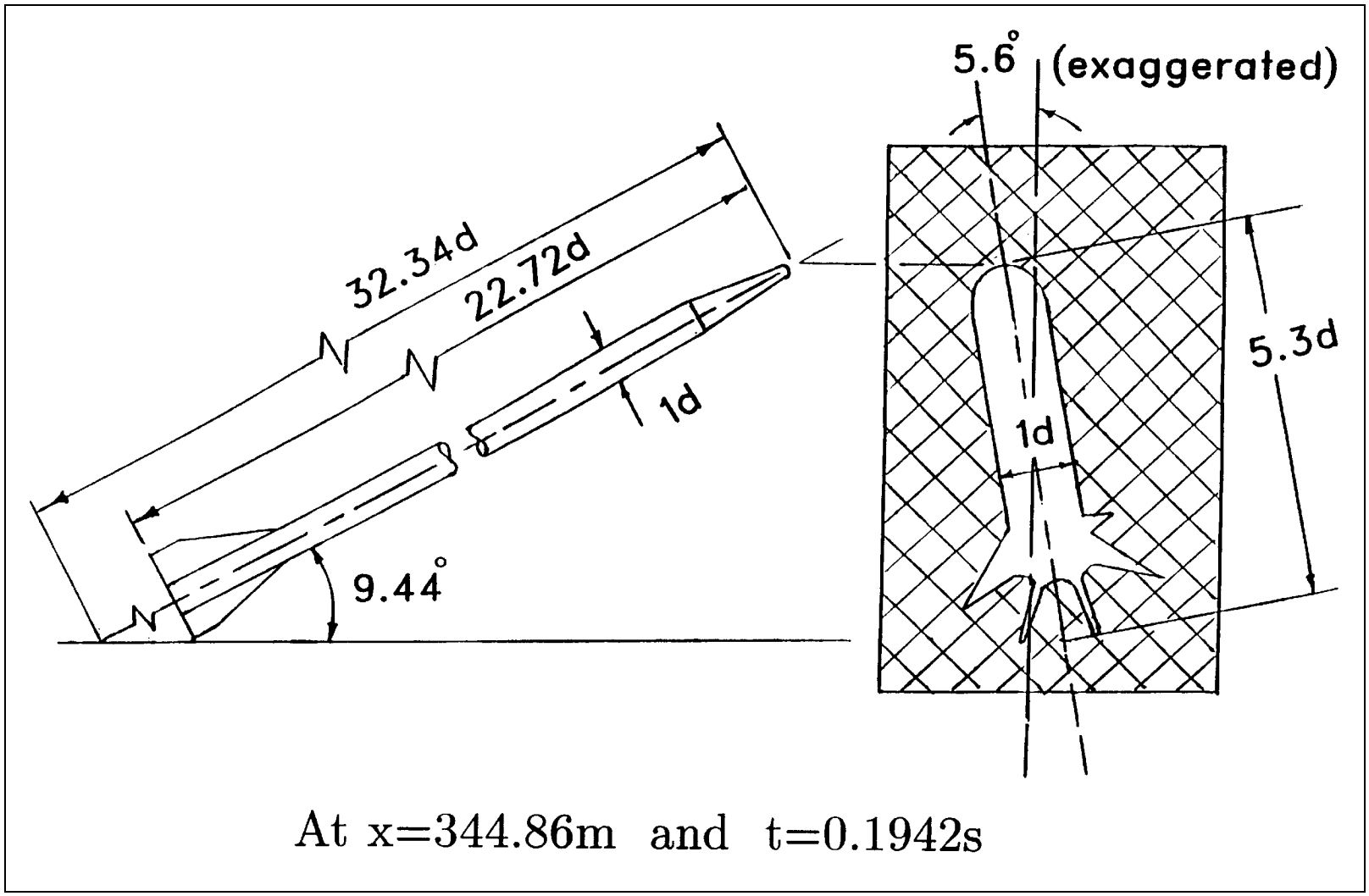

Figure 21. Predicted Impact Imprint of a Case of Roll/pitch Lock-in ($\delta_{eq} = 0.3\ \delta_d$, C_{Mo} = +1.222, and Δcg = 0.0).

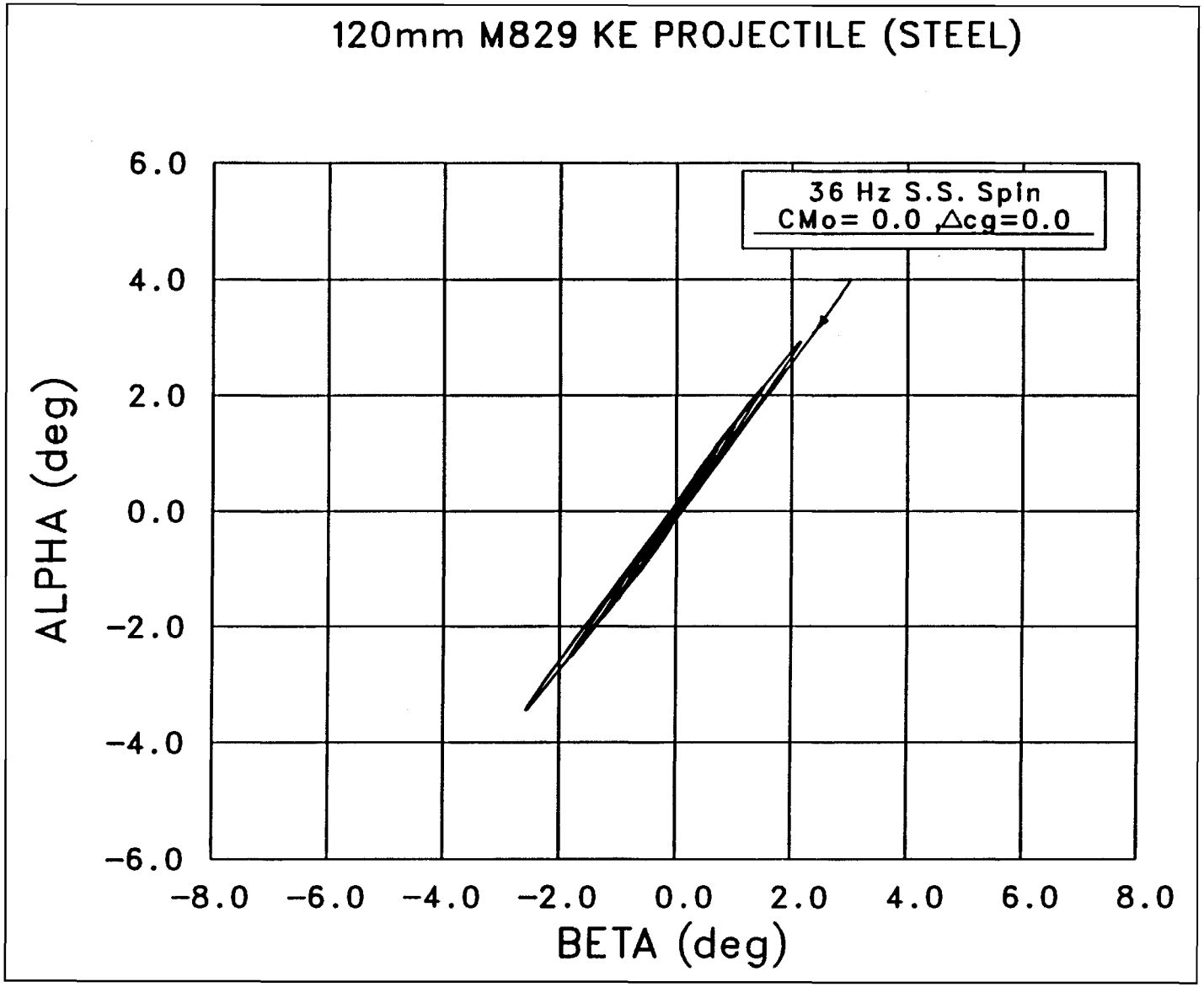

Figure 22. α - β Plot for a No-Lock-in Case ($\delta_{eq} = 0.4\ \delta_d$, C_{Mo} = -0.0, and Δcg = 0.0).

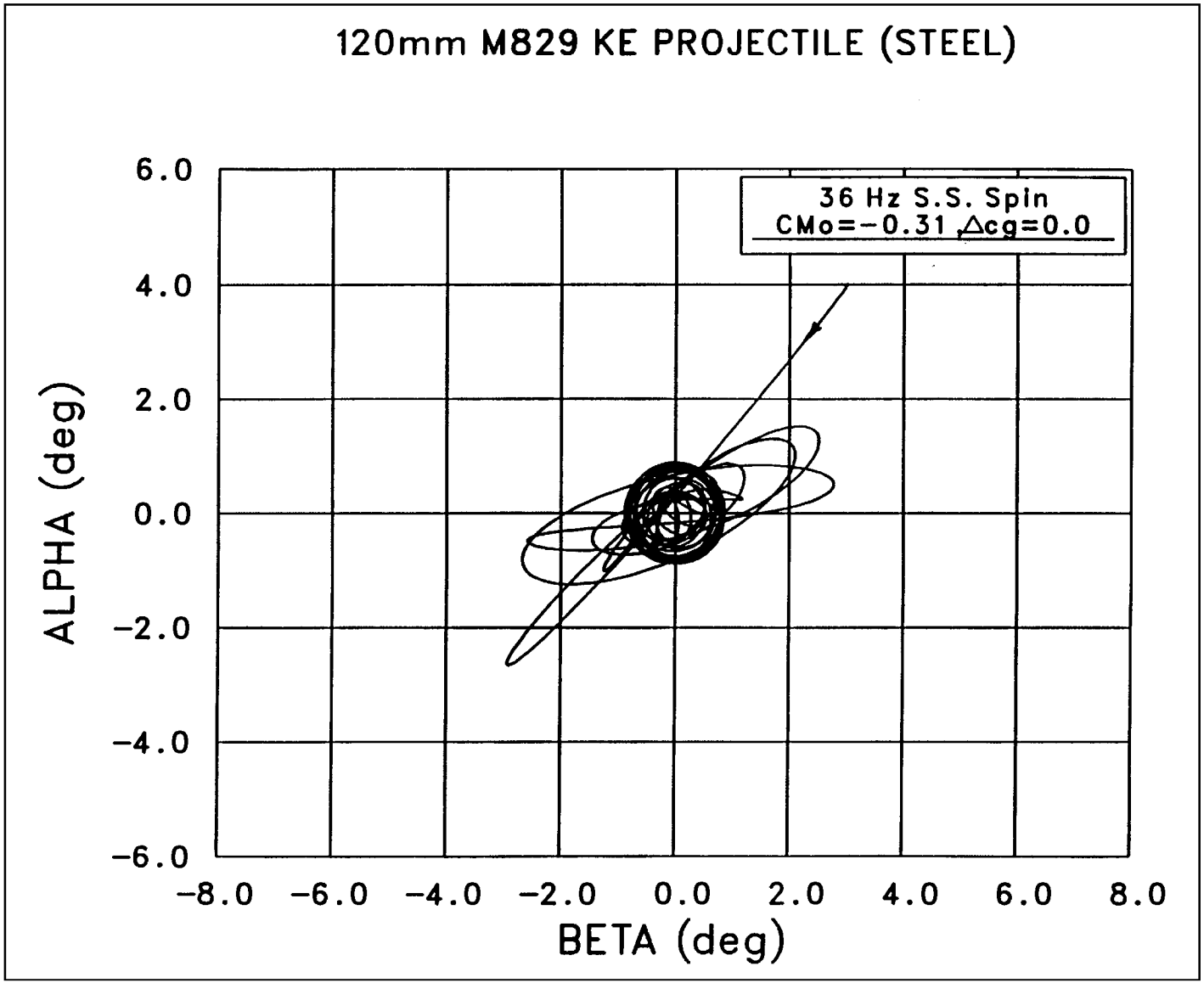

Figure 23. α - β Plot for a Case With Roll Resonance and Later Roll/pitch Lock-in ($\delta_{eq} = 0.4\ \delta_d$, C_{Mo} = +0.305, and Δcg = 0.0).

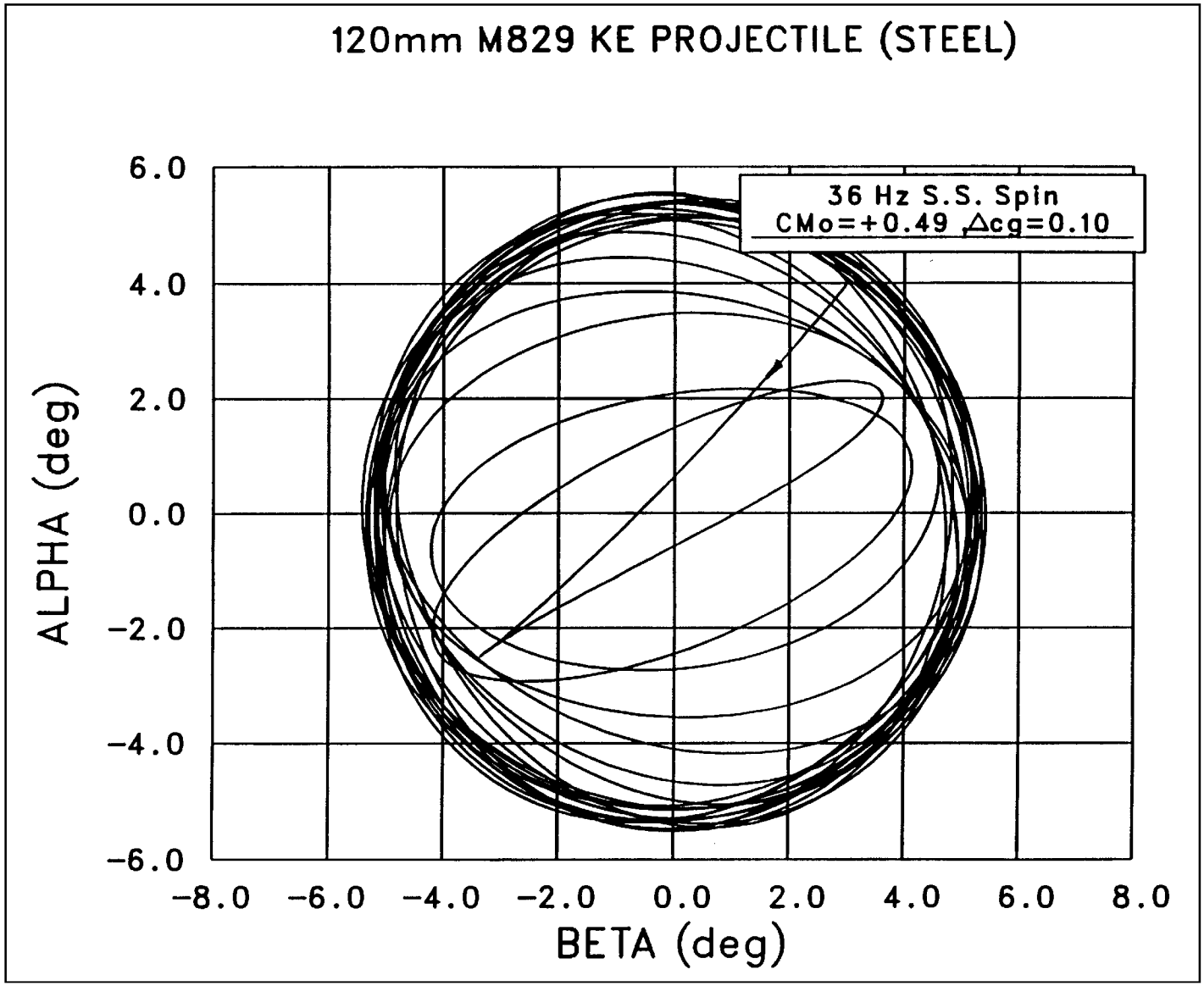

Figure 24. α - β Plot for a Lock-in Case ($\delta_{eq} = 0.4\ \delta_d$, $C_{Mo} = +0.489$, and $\Delta cg = 0.10$).

6. CONCLUSIONS AND SUMMARY

The following conclusions are supported by the results obtained through the application of the present analysis and model:

1. Fin area damage, in certain size and direction, can cause the lowering of the design steady state spin to a value close to the vehicle pitching motion frequency, thus creating the environment for possible locking in to that frequency.

2. It does not take a large fin damage to cause the low spin and therefore provides the condition for possible locking in at the pitching motion frequency. For the case studied for a six-finned projectile, a single fin panel idealized area damage of 10% of the fin area, bent at 19.2°, was enough to lower the spin and also cause the lock-in.

3. The higher or lower the expected steady state spin (attributable to damage) differs from the pitching motion frequency, the larger the mass offset needed to cause lock-in, in absence of fin asymmetry damage.

4. If the fin damage is less than that required to cause lock-in, the spinning motion will escape from being locked in but with some resonance effect on the spin history.

5. In case of mass offset alone, lock-in can also theoretically happen with no moment asymmetries ($C_{Mo} = 0.0$).

6. If a combination of both asymmetry moment and mass offset is causing the lock-in, their individual required magnitudes will be less than those required if each were to have been applied alone to cause a lock-in (confirming one's expectation).

In summary, a model was developed to study and simulate the roll and pitching motions lock-in observed for some projectiles in flight. Fin damage and mass offset were quantified and their effects on the motion of the vehicle were computed. Flight histories of the motion including the spin rate, pitch and yaw angles, and yaw amplification factor are computed. Both roll resonance and roll lock-in behavior were reflected in the flight histories computed. Projectile impact imprint on yaw cards is predicted and simulated for any distance from the muzzle. The model established is applicable for missiles or finned projectiles. A case study was performed in detail for a specific projectile, as a real-life applied example.

INTENTIONALLY LEFT BLANK

REFERENCES

1. Pennekamp, R. A. and Jara, E. A., "M900 Technical Test Results: Yaw and Spin Characterization Subtest," BRL-MR-3941, U.S. Army Ballistic Research Laboratory, Aberdeen Proving Ground, Maryland, December 1991.

2. Pennekamp, R. A., "M829A2 Technical Test Results: Yaw and Spin Characterization Subtest," ARL-MR-46, U.S. Army Research Laboratory, Aberdeen Proving Ground, Maryland, February 1993.

3. Nicolaides, J. D., "On the Free Flight Motion of Missile Having Slight Configurational Asymmetries," U.S. Army Ballistic Research Laboratory, Aberdeen Proving Ground, MD, BRL-Report 858, 1952; also Institute of Aeronautical Sciences Paper 395, 1952.

4. Price, D. A., Jr., "Sources, Mechanisms And Control of Roll Resonance For Sounding Rockets," Journal of Spacecraft and Rockets, Vol. 4, November 1967, pp. 1516-1525.

5. Clare, T. A., "Non-Linear Resonance Instability In The Flight Dynamics of Missiles," Ph.D. Dissertation, Department of Aerospace and Mechanical Engineering, University of Notre Dame, Indiana, June 1970.

6. Clare, T. A., "Resonance Instability for Finned Configurations Having Nonlinear Aerodynamic Properties," Journal of Spacecraft and Rockets, Vol. 8, No. 3, March 1971, pp. 278-283.

7. Murphy, C. H., "Free Flight Motion Of Symmetric Missiles," BRL Report 1216, U.S. Army Ballistic Research Laboratory, Aberdeen Proving Ground, MD, July 1963.

8. Murphy, C.H., "Some Special Cases of Spin-Yaw Lock-In," Journal of Guidance, Control, and Dynamics, Vol. 12, No. 6, Nov.-Dec. 1989, pp. 771-776.

9. Lin, T. C., Sproul, L. K., and Muskat, R., "Persistent Roll Resonance Induced by Missile/RV Aeroelastic Behavior," AIAA Paper No. 95-0065, January 1995.

10. Mikhail, A. G., "In-Flight Flexure and Spin Lock-In For Kinetic Energy Projectiles," Journal of Spacecraft and Rockets, Vol. 33, No. 5, September-October 1996, pp. 657664. (Also AIAA paper No. 95-3429)

11. Legner, H. H., Lo, E. Y., and Reinecke, W. G., "Hypervelocity Projectile Design Implications At High Fineness Ratio," AIAA Paper 95-0064, January 1995.

12. Oberkampf, W. L. and Nicolaides, J. D., "Aerodynamics of Finned Missiles at High Angle of Attack," AIAA Journal, Vol. 9, No. 12, Dec. 1971, pp. 2378-2384.

13. Arrow Tech Associates, " User Manual - PC PRODAS Code, Version 3.6," Arrow Tech Company, South Burlington, Vermont, 1991.

14. Pennekamp, R. A., and Garner, J. M., "A Technique for Assessing In-Bore Fin Damage," ARL-TR-1293, U.S. Army Research Laboratory, Aberdeen Proving Ground, MD, January 1997.

15. Weinacht, P., and Sturek, M.B. "Computation of the Roll Characteristics of the M829 Kinetic Energy Projectile and Comparison With Range Data." BRL-TR-3172, U.S. Army Ballistic Research Laboratory, Aberdeen Proving Ground, MD, November 1990.

16. Moore, F. G., Hymer, T. C., McInville, R. M., "The 1995 Version of The NSWCDD Aeroprediction Code: Part II- Computer Program User"s Guide and Listing," NSWCDD/TR95/5, Naval Surface Warfare Center, Dahlgren Division, Dahlgren, Virginia, March 1995.

17. Erline, T. F., "Lateral Projectile Dynamics: M829 Projectile- Style vs. Puller Sabot," ARL-TR-630, U.S. Army Research Laboratory, Aberdeen Proving Ground, Maryland, November 1994.

LIST OF SYMBOLS

A_d = damaged area of a fin panel, in.^{2}
A_f = area for one single fin panel, in.^{2}
A_{ref} = reference area (π d^2/4), in.^{2}
C_D = drag coefficient, drag force/(0.5ρ_∞ = V_∞^2 A$_{\text{ref}}$)
Δcg = mass offset radial distance from body center, in.
C_l = rolling moment coefficient, I/(q_∞ A$_{\text{ref}}$d)
C_{li} = induced roll moment coefficient, Equation (1)
C_{lp} = roll moment damping coefficient derivative, $\partial C_l / \partial (pd/V)$, per radian
$C_{l\delta}$ = fin produced roll moment coefficient derivative, $\partial C_l / \partial \delta$, per radian
C_N = normal force coefficient, normal force/(q_∞ A$_{\text{ref}}$)
$C_{N\alpha}$ = normal force slope coefficient, ∂C_N / $\partial \alpha$, per radian
C_M = pitching moment coefficient, pitching moment/(q_∞ A$_{\text{ref}}$d)
C_{Mo} = asymmetry pitching moment coefficient
$C_{M\alpha}$ = pitching moment slope coefficient, ∂C_M / $\partial \alpha$, per radian
d = projectile reference diameter, in.
I_x = axial (polar) moment of inertia about the body spin axis, lb-in.^{2}
I_y = transverse moment of inertia about an axis passing through the body center of mass, lb-in.^{2}
l = roll moment, lb-in.
L = total length of the projectile, in.
M = Mach number of the projectile
n = number of fins in a fin set
n_d = number of damaged fins in a fin set
p = spin rate of projectile, rad/s (except where otherwise noted in Hz)
$q\infty$ = dynamic pressure, (0.5ρ V^2), psi
Δt = time step for numerical integration, s
V = projectile velocity, ft/s

Greek Symbols

α = body pitching angle of attack, deg
$\dot{\alpha}$ = dα / dt
α_t = total angle of attack (yaw) $\left(=\sqrt{\alpha^2+\beta^2}\right)$, deg
β = body side slip angle of attack, deg
δ_{eq} = equivalent fin cant angle for a whole fin panel for the partially canted (chamfered) fin, deg
δ_d = design value of the fin cant angle, deg
δ_{dg} = value of the fin cant damage angle, deg
$\delta_1, \delta_2, \delta_3$ = angles of the damaged area of the fin panel, deg

$\Delta_1, \Delta_2, \Delta_3$ = fin damage parameters: deg, deg, and inch, respectively

γ = fin plane roll orientation angle with respect to the plane of angle of attack, deg

Γ = initial angle of mass offset location, deg

λ = angle of the C_{Mo} asymmetry moment, deg

ρ = air density, slug/ft^3

ϕ = roll angle, radian

$\dot{\phi}$ = roll (spin) rate, dϕ/dt, rad/s (except otherwise noted in Hz)

ω_n = first natural frequency in lateral bending, rad/s

ω_p = pitching motion frequency, $\sqrt{\left(-C_{M\alpha} q A_{ref} d / I_y\right)}$, rad/s

NO. OF COPIES ORGANIZATION

2 ADMINISTRATOR
DEFENSE TECH INFO CENTER
ATTN DTIC OCP
8725 JOHN J KINGMAN RD STE 0944
FT BELVOIR VA 22060-6218

1 DIRECTOR
US ARMY RESEARCH LABORATORY
ATTN AMSRL CS AL TA
RECORDS MANAGEMENT
2800 POWDER MILL RD
ADELPHI MD 20783-1197

1 DIRECTOR
US ARMY RESEARCH LABORATORY
ATTN AMSRL CI LL
TECHNICAL LIBRARY
2800 POWDER MILL RD
ADELPHI MD 207830-1197

1 DIRECTOR
US ARMY RESEARCH LABORATORY
ATTN AMSRL D R W WHALIN
2800 POWDER MILL RD
ADELPHI MD 20783-1197

1 DIRECTOR
US ARMY RESEARCH LABORATORY
ATTN AMSRL DD J J ROCCHIO
2800 POWDER MILL RD
ADELPHI MD 20783-1197

11 CDR US ARMAMENT RD&E CENTER
ATTN AMSTA AR AET A/C NG
AMSTA AR AET A/J GRAU
AAMSTA AR AET A/S KAHN
AAMSTA AR AET A/H HUDGINS
AAMSTRA AR AET A
M AMORUSO
AAMSTA AR AET A/E BROWN
AAMSTRA AR AET A/B WONG
AAMSTA AR AET A/W TOLEDO
AAMSTA AR AET A/S CHUNG
AAMSTA AR AET A
C LIVECCHIA
AAMSTA AR AET A G MALEJKO
PICATINNY ARSENAL NJ 07806-5000

3 COMMANDER
US ARMAMENT RD&E CENTER
ATTN AMSTA AR CCH B/B KONARD
AMSTA AR CCH B/E FENNELL
AMSTA AR CCH B/T LOUZEIRO
PICATINNY ARSENAL NJ 07806-5000

NO. OF COPIES ORGANIZATION

4 COMMANDER
US ARMAMENT RD&E CENTER
ATTN AMSTA AR FSE/A GRAF
AMSTA AR FSE/D LADD
AMSTA AR FSE E ANDRICOPOULIS
AMSTA AR FSE/K CHEUNG
PICATINNY ARSENAL NJ 07806-5000

6 COMMANDER
US ARMAMENT RD&E CENTER
ATTN AMSTA AR CCL D/F PUZYCKI
AMSTA AR CCL D/D CONWAY
AMSTA AR CCL D/D DAVIS
AMSTA AR CCL D/K HAYES
AMSTA AR CCL D/M PINCAY
AMSTA AR CCL D/W SCHUPP
PICATINNY ARSENAL NJ 07806-5000

2 PROJECT MANAGER
TANK MAIN ARMAMENT SYSTEM
ATTN SFAE ASM TMA/MAJ B HELD
SFAE ASM TMA/R KOWALSKI
PICATINNY ARSENAL NJ 07806-5000

3 US ARMY RESEARCH OFFICE
ATTN G ANDERSON K CLARK
T DOLIGOWSKI
PO BOX 12211
RSCH TRIANGLE PARK NC 27709-2211

2 US ARMY BENET LABORATORY
ATTN SMCAR CCB R/S SOPOK
SMCAR CCB R/P ALTO
WATERVALIET NY 12189

3 COMMANDER
US NAVAL SURFACE WARFARE CTR
ATTN CODE DK20 (CLARE)
CODE DK20 (MOORE)
CODE DK20 (DEVAN)
DAHLGREN VA 22448-5000

2 COMMANDER
US NAVAL SURFACE WARFARE CTR
ATTN CODE R44 A WARDLAW
CODE R44 F PRIOLO
WHITE OAK LABORATORY
SILVER SPRING MD 20903-5000

1 DIRECTOR
NASA AMES RESEARCH CENTER
ATTN MS 258 1 L SCHIFF

MOFFETT FIELD CA 94035

NO. OF COPIES	ORGANIZATION
2	DIRECTOR SANDIA NATIONAL LABORATORIES ATTN W OBERKAMPF W WOLFE DIVISION 1636 P O BOX 5800 ALBUQUERQUE NM 87185
1	COMMANDER US ARMY MISSILE COMMAND ATTN AMSMI RD SS AT/W WALKER REDSTONE ARSENAL AL 35898-5010
2	NASA LANGLEY RESEARCH CENTER ATTN TECH LIBRARY M HEMSCH LANGLEY STATION HAMPTON VA 23665
3	AIR FORCE ARMAMENT LABORATORY ATTN AFATL FXA/B SIMPSON G ABATE R ADELGREN EGLIN AFB FL 32542-5434
1	LOS ALAMOS NATL LABORATORY ATTN MS G770/W HOGAN LOS ALAMOS NM 87545
1	DIRECTOR DEF ADV RSCH PROJECTS AGENCY ATTN TACTICAL TECHNOLOGY OFC 1400 WILSON BOULEVARD ARLINGTON VA 22209
1	US MILITARY ACADEMY DEPT OF MATHEMATICS ATTN M J GRAHAM WEST POINT NY 10996
1	CECOM SP & TERRESTRIAL COM DIV ATTN AMSEL RD ST MC M H SOICHER FT MONMOUTH NJ 07703-5203
1	CECOM ATTN PM GPS COL S YOUNG FT MONMOUTH NJ 07703
1	ODCSOPS D SCHMIDT WASHINGTON DC 20310-1001

NO. OF COPIES	ORGANIZATION
1	OSD ATTN OUSD(A&T)/ODDDR&E(R) ATTN R J TREW WASHINGTON DC 20301-7100
1	ARL ELECTROMAG GROUP CAMPUS MAIL CODE F0250 A TUCKER UNIVERSITY OF TEXAS AUSTIN TX 78712
1	DARPA ATTN B KASPAR 3701 N FAIRFAX DR ARLINGTON VA 22203-1714
1	SPECIAL ASST TO THE WING CDR 50SW/CCX CAPT P H BERNSTEIN 300 O'MALLEY AVE STE 20 FALCON AFB CO 80912-3020

ABERDEEN PROVING GROUND

2	DIRECTOR US ARMY RESEARCH LABORATORY ATTN AMSRL CI LP (TECH LIB) BLDG 305 APG AA
2	COMMANDER US ARMY ABERDEEN TEST CENTER ATTN STECS EN PM/J FALLER STECS EN PM/D HORTON BLDG 400 APG-AA
2	COMMANDER US ARMAMENT RD&E CENTER ATTN AMSTA AR FSF T R LIESKE F MIRABELLE BLDG 120 APG-AA
1	DIRECTOR US ARMY RESEARCH LABORATORY ATTN AMSRL WM DR I MAY BLDG 4600
1	DIR USARL ATTN AMSRL WM B A W HORST JR BLDG 4600
1	DIR USARL ATTN AMSRL WM B E M SCHMIDT BLDG 309A

ALEXANDRIA VA 22333-0001

NO. OF COPIES	ORGANIZATION
1	DIR ARL ATTN AMSRL WM BA F BRANDON BLDG 4600
15	DIR USARL ATTN AMSRL WM BC P PLOSTINS M BUNDY G COOPER H EDGE B GUIDOS D LYON A MIKHAIL (5 CYS) J SAHU K SOENCKSEN D WEBB A ZIELINSKI BLDG 390
2	DIR USARL ATTN AMSRL WM BC J GARNER V OSKAY BLDG 740B
1	DIR USARL AMSRL WM BE DR T MINOR BLDG 390
1	DIR USARL AMSRL WM MB B BURNS BLDG 4600
	ABSTRACT ONLY
1	DIRECTOR US ARMY RESEARCH LABORATORY ATTN AMSRL CS AL TP TECH PUB BR 2800 POWDER MILL RD ADELPHI MD 20783-1197
1	COMMANDER US ARMY MATERIEL COMMAND ATTN AMCRDA TF 5001 EISENHOWER AVENUE ALEXANDRIA VA 22333-0001
1	PRIN DPTY FOR TECH GY HDQ US ARMY MATL CMND ATTN AMCDCG T 5001 EISENHOWER AVE ALEXANDRIA VA 22333-0001
1	PRIN DPTY FOR ACQTN HDQ US ARMY MATL CMND ATTN AMCDCG A 5001 EISENHOWER AVE

NO. OF COPIES	ORGANIZATION
1	DPTY CG FOR RDE HDQ US ARMY MATL CMND ATTN AMCRD BG BEAUCHAMP 5001 EISENHOWER AVE ALEXANDRIA VA 22333-0001
1	COMMANDER US ARMY MATERIEL COMMAND ATTN AMCDE AQ 5001 EISENHOWER AVENUE ALEXANDRIA VA 22333-0001

INTENTIONALLY LEFT BLANK

REPORT DOCUMENTATION PAGE

Form Approved
OMB No. 0704-0188

1. AGENCY USE ONLY *(Leave blank)*	2. REPORT DATE	3. REPORT TYPE AND DATES COVERED
	November 1997	Final

4. TITLE AND SUBTITLE

Fin Damage and Rod Eccentricity for Spin/Pitch Lock-in for Antiarmor Kinetic Energy Projectiles

5. FUNDING NUMBERS

PR: 1L162618AH80

6. AUTHOR(S)

Mikhail, A.G. (ARL)

7. PERFORMING ORGANIZATION NAME(S) AND ADDRESS(ES)

U.S. Army Research Laboratory
Weapons & Materials Research Directorate
Aberdeen Proving Ground, MD 21010-5066

8. PERFORMING ORGANIZATION REPORT NUMBER

9. SPONSORING/MONITORING AGENCY NAME(S) AND ADDRESS(ES)

U.S. Army Research Laboratory
Weapons & Materials Research Directorate
Aberdeen Proving Ground, MD 21010-5066

10. SPONSORING/MONITORING AGENCY REPORT NUMBER

ARL-TR-1442

11. SUPPLEMENTARY NOTES

12a. DISTRIBUTION/AVAILABILITY STATEMENT

Approved for public release; distribution is unlimited.

12b. DISTRIBUTION CODE

13. ABSTRACT *(Maximum 200 words)*

A study and a general model for the roll/pitch frequency "lock-in" phenomenon are made for antitank long kinetic energy projectiles and missiles in general, to quantify the necessary projectile damage/defect required to cause the lock-in. (Lock-in is a "persistent" resonance for the flight duration of the vehicle [i.e., projectile].) Fin damage and body mass offset are modeled as the forcing forces and moments (asymmetries) causing the lock-in. Idealized fin damage is modeled. The corresponding pitch, side slip, and roll equations are numerically integrated. The resulting yaw is largest when the projectile is spinning near the pitching frequency, and yaw diminishes when the spin rate (attributable to fin damage) is away from it. The nonlinear induced roll moment is essential in coupling the pitching/yawing motions with the moment of the roll motion. A specific and complete projectile case study is presented, in which quantified fin damage and rod mass offset are found to cause such lock-in. Computed flight motion history (pitch, side slip, and roll), and yaw amplification factor provide insight into this lock-in behavior. The model is general and can be applied to any finned projectile or missile.

14. SUBJECT TERMS

analysis, KE projectiles, spin lock-in, fin damage, rod eccentricity

15. NUMBER OF PAGES

60

16. PRICE CODE

17. SECURITY CLASSIFICATION OF REPORT	18. SECURITY CLASSIFICATION OF THIS PAGE	19. SECURITY CLASSIFICATION OF ABSTRACT	20. LIMITATION OF ABSTRACT
Unclassified	Unclassified	Unclassified	